High power all-carbon fully printed and wearable SWCNT-based organic thermoelectric generator

Christos K. Mytafides [*][❖]*, Lazaros Tzounis* [**][❖]*, George Karalis* [❖]*, Petr Formanek* [§] *and Alkiviadis S. Paipetis* [***][❖]

[❖] Department of Materials Science & Engineering, University of Ioannina, GR-45110 Ioannina, Greece

[§] Leibniz-Institut für Polymerforschung Dresden e.V., Hohe Straße 6, 01069 Dresden, Germany

ABSTRACT

In this study, we introduce the fabrication process of a highly efficient fully printed all-carbon Organic Thermoelectric Generator (OTEG) free of metallic junctions, with outstanding flexibility and exceptional power output, which can be conveniently and rapidly prepared through ink dispensing/printing processes of non-toxic and low-cost aqueous CNT inks with a mask-assisted specified circuit architecture. The optimal produced p-type and n-type films exhibit ultrahigh power factors of 308 $\mu W/mK^2$ and 258 $\mu W/mK^2$ respectively at $\Delta T=150K$ ($T_{HOT}=175°C$) and outstanding stability in air without encapsulation, providing the OTEG device the ability to operate at high temperatures up to 200°C at ambient conditions (1 atm, relative humidity: 50±5% RH). We have successfully design and fabricate the flexible thermoelectric modules with superior thermoelectric properties of p-type and n-type SWCNT films resulting in exceptionally high performance. The novel-design OTEG exhibits outstanding flexibility and stability with attained TE values among the highest ever reported in the field of organic thermoelectrics, i.e. open-circuit voltage V_{OC}= 1.05 V and short-circuit current I_{SC}= 1.30 mA at ΔT= 150 K ($T_{HOT}=175°C$) with an

internal resistance of R_{TEG}= 806 Ω, generating 342 µW power output. It is also worth noting the remarkable power factors of 145 µW/mK^2 and 127 µW/mK^2 for the p-type and n-type films respectively at room temperature. The fabricated device is highly scalable, providing opportunities for printable large-scale manufacturing/industrial production of highly efficient flexible OTEGs.

TOC GRAPHICS
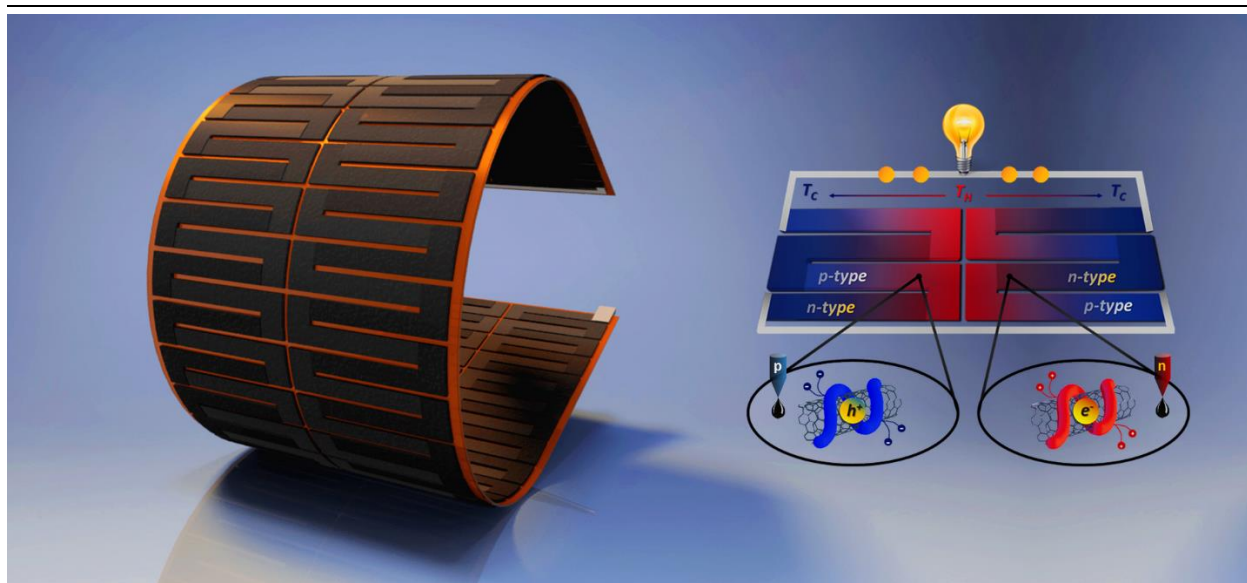
Graphical abstract. Schematic illustration of the all-carbon printed and flexible SWCNT-based organic thermoelectric generator

1. INTRODUCTION

Energy conversion from primary energy carriers into end-use energy is subject to losses. Massive quantities of converted energy are usually released to the environment as waste heat. The exploitation of this waste energy may increase energy efficiency and reduce energy consumption. Waste heat produced globally by the most common end-use sectors including transportation, industrial, commercial & residential as well as electricity generation on a global scale, it is estimated at 72% of the global primary energy consumption. In more detail, 63% of the aforementioned waste energy concerns temperatures below 100 °C. In this temperature range,

electricity generation sector has the largest share followed by transportation and industry [1]. Thermoelectric (TE) energy harvesting is an emerging and promising technology of renewables in a wide range of applications. TE materials convert heat directly into electricity and may be employed for harvesting dissipated heat, local cooling, and more recently flexible and wearable electronics [2-8]. Although TE conversion devices offers a theoretically effective and sustainable energy harvesting solution from waste heat sources for a wide range of temperatures, most of the semiconductors that currently deliver the best TE performance are expensive to manufacture and are based on relatively rare and/or toxic elements. The most commonly used thermoelectric materials are inorganic semiconductors and their alloys, i.e. Bi_2Te_3, Sb_2Te_3 and $PbTe$ [9]. Therefore, the cost per watt of generated electricity becomes prohibitively expensive, which is consistent with the fact that there is no significant commercial market for TE converters. A potential application for TEG devices is the power generation in distant locations, and the power supply for portable wireless devices with low power requirements (e.g. health sensors, Internet of Things). In order to achieve this applicability, the form factor and the weight of the device (e.g. adaptability and flexibility) become just as essential as the cost and efficiency. This creates the demand for simple process such as those based on non-toxic, low-cost organic (or hybrid) semiconducting TE inks, which can be deposited onto flexible substrates for the production of flexible TE materials [10]. In recent years, organic and organic/inorganic composite TE materials have attracted considerable scientific interest due to their numerous advantages, i.e. low cost, low density, non-toxic, low thermal conductivity and facile processing [11-13].

The establishment of organic TE materials in the renewables market as a meaningful player towards global sustainable energy solutions is largely dependent on the production of cost-effective and environmental-friendly TE materials. Carbon nanotubes (CNT), [14-16], conductive

polymers [17-20], or CNT/polymer composites [21-30], are materials with excellent properties that may also be tailored on demand and therefore offer extensive design-based application opportunities [31]. Although significant progress has been made on p-type organic TE materials, the optimized design of high-performance and air-stable flexible n-type organic TE materials to match their p-type counterparts and further increase the energy conversion capacity of TEG devices remains a major challenge [32-35]. The main reason is the shortage of solution-processable n-type dopants for organic TE materials with long-term environmental stability. Furthermore, air-stable n-type organic TE materials with inherent flexibility are not yet as efficient to produce TE generators and optimize their performance. This is generally the case for printable and flexible n-type materials where high-performance is also essential for applications such as organic solar cells [36] or field-effect transistors [31, 37, 38]. SWCNTs, are promising as an emerging TE material, because they exhibit extraordinary TE characteristics together with excellent and highly tuned performance via ion or molecular doping [29, 31, 39-48]. Pristine SWCNTs possess a p-type character due to oxygen impurities in the atmosphere [31, 39]. Through specific doping methods with organic small molecules or polymers with electron donors or acceptors , SWCNTs can be engineered to either p-type [40-42], or n-type [29, 43-50] materials where the major inherent carriers are positively or negatively charged respectively. Trailblazer SWCNT n-doping research is based on polyethyleneimine (PEI), [43, 44] and organic molecules of electron donors (e.g. nitrogen or phosphine-containing dopants) [29]. Additionally, a series of amines (e.g. amino-substituted rylene dimides, diethylenetriamine) and ordinary salts (e.g. NaCl, NaOH, KOH) with crown ethers were found to be suitable as n-type dopants of CNTs [29, 30, 45]. However, the above-mentioned doping methods, give rise to high-cost, unstable in air and even dangerous inks, which are not easy processable, or non-water-soluble. All of the above, underline the need for simple, high-performance and low-cost n-type SWCNTs [46]. The power

factor (PF) is often employed to characterise TE materials and is defined as $PF = \sigma \cdot S^2$ where S is the Seebeck coefficient and σ is the electrical conductivity of a TE material [51].

Although it is often reported that TEG devices formed with high power factor materials are able to generate more energy, this is only the case for TEGs with well-specified geometries without any constraints of heating and cooling. For an application-based optimally designed TEG, the employed TE materials should work at their peak efficiency, which is determined by their figure of merit $ZT = \sigma \cdot S^2 \cdot T / \kappa$, [52], where T is the absolute temperature and κ the thermal conductivity. In a very first study related to n-type organic TE materials published by Sun et al. [10], the metallic coordination n-type polymer poly(K_x(Ni-ett)) has shown sufficient TE characteristics, with a PF of 66 $\mu W/mK^2$. In addition, CNTs are highly promising organic materials which can be easily adapted to n-type by different methods such as electron-rich polymer functionalization [30, 38, 53, 54], metal encapsulation [28, 55], conjugated polyelectrolytes [27] and small molecules [29]. In previous studies, n-type TE films based on dispersed CNT solutions with the addition of PEI as n-dopant, have resulted in low electrical conductivity and a conservative PF (maximum PF=72 $\mu W/mK^2$) [28, 31, 56]. In a more relevant study to this one, ammonium-based cationic surfactants were employed as n-dopants to SWCNTs to achieve a reasonably high PF=100 $\mu W/mK^2$ using CTAB in H_2O solvent [57].

In this study, we develop non-toxic, facile, low-cost, high-temperature resistant, air-stable and flexible p- and n-type SWCNT-based TE films. The produced n-type films exhibit an ultrahigh TE PF of ~258 $\mu W/mK^2$ and an outstanding long-term stability in air without encapsulation at $\Delta T = 150K$. We demonstrate that SWCNTs can easily be dispersed in water, resulting to n-type ink via a simple solution mixing procedure, with the addition of the small molecule of cetyltrimethylammonium bromide (CTAB). CTAB is a common alkylammonium cationic

surfactant, giving the ability to dope efficiently the SWCNT with electrons, as well as to disperse them into a water solution, which provides a great opportunity for printable, large-scale roll-to-roll (R2R) or sheet-to-sheet (S2S) industrial production. Inspired by these results, we successfully design and fabricate a fully printed and powerful OTEG device on a kapton film, consisting of serially interconnected p- and n-type SWCNT thermoelements, demonstrating impressive performance, stability, and flexibility, capable to produce power at high temperatures up to 200 ºC. The flexible novel-design OTEG device consisting of 116 p-/n- pairs can generate the remarkable total thermopower of 7791 μV/K at $\Delta T=100K$ ($T_C=25°C$, $T_H=125°C$). Furthermore, exceptional values for open-circuit voltage $V_{OC}=1.05$ V and short-circuit current $I_{SC}=1.30$ mA were achieved at $\Delta T=150$ K ($T_H=175°C$) with an internal resistance $R_{TEG}=806$ Ω, resulting to the ultra-high power output of 342 μW.

2. EXPERIMENTAL SECTION

2.1. Characterization techniques

The LabRAM HR800 Horiba scientific micro-Raman system (Horiba, Japan) was used in order to verify the purity and crystallinity of SWCNT-based thermoelectric materials. A 514.5 nm Ar^+ ion laser with 1.0 mW operating power at the focal plane was employed for the Raman excitation. An optical microscope equipped with a 100× objective served both for delivering the excitation light and collecting the back-scattered Raman activity. All Raman spectra were collected in the range of 90-3500 cm^{-1} with acquisition times of 30 s. Viscosity measurements of the TE inks have been carried out with the NDJ-9S digital viscometer. The UV-3600, Shimadzu ultraviolet–visible–near infrared (NIR) spectrophotometer (Shimadzu, Japan) was used in order to measure the absorption spectra. Microscopic morphology was characterised using a FIBSEM Zeiss-Neon 40EsB focused ion beam-scanning electron microscope (Zeiss, Germany) operating at an accelerating voltage of

3.0–5.0 kV. Furthermore, the Bruker Innova Atomic Force Microscope (Bruker, USA) was used in order to characterise the surface morphology of the printed TE films, operating at 3V using Antimony doped Si probe (RTESPA-300) with f_0=300kHz at tapping mode.

2.2. Measurements of TE properties and performance

The TE related properties of the materials, including Seebeck coefficient, electrical conductivity, thermal conductivity, power factor, figure of merit and thermoelectric efficiency were measured using the Linseis Thin Film Analyzer (Linseis, Germany). Ossila 4-point probe instrument was also used for the determination of the sheet resistance and the electrical conductivity of the films (Ossila, United Kingdom). Thermal stability and performance of the materials and the TEG device were carried out. In order to generate thermopower, one block was kept at room temperature ($T_C \simeq 25°C$) and the other was heated at various temperatures (laboratory environment: 1 atm, relative humidity: 50±5% RH). The temperature of the two blocks was monitored with K-type thermocouples to accurately determine the temperature difference (ΔT). The generated voltage and current in various ΔTs were measured using the Agilent 34401A digital multimeter (Agilent Technologies, USA) and DMM connectivity utility software. The TE performance evaluation system employed for the flexible module provided the voltage–current, power–current, voltage–load resistance and power–load resistance curves was computer-controlled by purposely made LabVIEW programmes. The thermal behavior of the SWCNT-based TE materials was investigated by thermogravimetric analysis (TGA) using a Leco TGA701 instrument (Leco, USA). Thermal scans were performed under oxygen flow from 30 °C to 1000 °C with a heating rate of 10 °C/min. C.K.M. participated in the thermoelectric characterization of the wearable OTEG device at his own responsibility without any permission due to the non-toxic environmentally friendly materials that have been used for the fabricated OTEG.

3. FABRICATION PROCESS OF THE ORGANIC THERMOELECTRIC GENERATOR

3.1. Preparation of p- and n-type SWCNT-based TE inks

The pristine SWCNT powder with a carbon purity of ≥80% has been obtained from TUBALL™, (OCSiAl , Russia) with a length of ca. 5µm and outer mean diameter of 1.6 ±0.4 nm. The p-type SWCNT ink was fabricated by an easy water-solution mixing procedure, with the addition of anionic surfactant sodium dodecylbenzene sulfonate (SDBS) and SWCNTs in deionized water (DI water). The mixture of 2mg/ml SWCNTs with a prescribed amount of SDBS in 100ml H_2O was initially stirred for 10 min, then tip-sonicated for 30 min using a Hielscher-UP400S probe-type sonicator (Hielscher, Germany), stirred for 15 min, tip-sonicated for another 30 min and finally stirred for 3h. All stirring processes carried out at 1000 rpm and the tip-sonication at 10W. In order to produce high-quality printable TE inks with high performance, it is of great importance to produce high-quality dispersions with the appropriate viscosity depending on the design, the application and the substrate [58, 59]. In this work, the desired viscosity for the printing process is approximately 350 cP, and was achieved for the dominant dispersions [58, 60].

During the dispersion process, it has been observed that the lower the SDBS addition to the p-type ink, the greater the conductivity of the mixture and, as a result, the power factor of the material. However, very low amounts of SDBS do not contribute to good dispersion of CNTs, resulting in a low-quality TE ink forming discontinuous films with low conductivity, not suitable for large-scale applications.

The n-type SWCNT ink is fabricated using a facile, low-cost and fast water-solution procedure, mixing CTAB and SWCNTs in DI water, in a similar way as for the SDBS process described above. In this work, cetyltrimethylammonium bromide (CTAB) as a typical and one of the most

commonly used alkylammonium cationic surfactant, was studied as a low-cost, high-temperature, air-stable and non-toxic n-dopant. SDBS as well as CTAB powders were obtained from Sigma-Aldrich (Steinheim, Germany). Figure 1 illustrates the manufacturing process of the TE inks, the dispersions of p- and n-type SWCNTs, the printed TE thin films for the thermoelectric characterisation, the vacuum filtration for buckypaper fabrication as well as the outstanding flexibility of p- and n-type SWCNT buckypaper films.
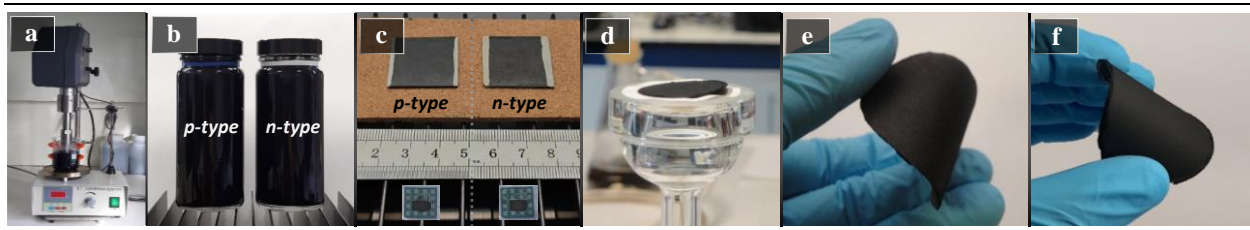

Figure 1. Thermoelectric ink preparation for material characterisation. (a) The dispersion process using a probe-type sonicator, (b) the as prepared dispersions of p- and n-type SWCNTs, (c) the TE thin films for the thermoelectric characterisation, (d) the vacuum filtration process for buckypaper preparation and (e-f) the outstanding flexibility of p- and n-type SWCNT buckypaper films respectively.

3.2. Fabrication of the flexible OTEG

A flexible all-carbon TEG module was fabricated via ink dispensing/ printing method with the manufactured TE inks on a high temperature resistant Kapton thin-film (~100μm thickness) and consisted of 116 p-/n- pairs. Figure 2 depicts the mask-assisted device fabrication process with dimensions of 30 cm × 7 cm × 110 μm, as well as the outstanding flexibility of the OTEG device. Initially, p-type TE material was printed on the flexible Kapton substrate by blade-coating technique. The blade was set at 2.5mm wet film thickness, resulting in homogenous 5μm dry film thickness of the SWCNT-based TE material. Subsequently, n-type TE material was printed in the same way so that it met the p-type thermal element where it ended, in order to create a continuous electric path consisting of p-/n- thermoelements. In an attempt to visualize the SWCNT film

thickness printed onto the Kapton substrate (representative of the SWCNT thickness of the TEG printed device consisting thermoelements), ultrasmooth block surfaces were prepared using an ultramicrotome (Leica UC7, Leica Microsystems GmbH, Wetzlar, Germany) and a diamond knife for polishing (model cryotrim 45°) under cryo conditions (−120 °C). Prior to the SEM analysis, a thin layer (3 nm) of platinum was deposited by sputtering in order to avoid charging effects. Supplementary Figure 8 illustrates the cross-section of the printed film. The dimensions of each thermoelement were 2.5 cm × 0.4 cm × 5 μm. The thermoelements were dried at 90 °C for 20 min after printing. In this configuration, the highly conductive SWCNT networks are also employed as electrodes/ interconnections between the p-/n- regions, thereby forming an all-carbon TEG without the need for additional metal deposition for electrical interconnection of the thermoelements. In order to maximise the filling factor as well as the power output of the device, the OTEG architecture was mirror printed for both sides of the Kapton substrate. The SI-P2000 nanosilver ink ORGACON™ that has been obtained from AGFA (AGFA, Belgium), was only used for the interconnection between the both-side printed pattern of thermoelements as shown in Figure 2a. In this case, the Ag-paste was applied on the Kapton substrate via mask-assisted printing process and dried at 150 °C for 20 min prior to the printing of the thermoelements with TE inks.

Most CNT-based TEGs are fabricated via p- and n-type alternating stacking (or printing) of the thermoelements using metal deposition for electrical interconnection [51, 57]. However, in the case of highly electrically conductive SWCNTs, the contact resistance between the metal electrode and the SWCNTs is higher than the resistance of the metal or the SWCNT itself and, as a result, this method yields TEGs with reduced power output [61]. Supplementary Figure 1 illustrates an Ag-interconnected TEG with the same architecture as the fabricated OTEG and Supplementary Figure 2 shows its thermoelectric performance under ΔT:100K (Tc=25°C).

In this study, we demonstrate the facile fabrication of a flexible, non-toxic and fully printed all-carbon TEG device. The employed SWCNT-based printed films have excellent electrical conductivities of 1956 S/cm and 1351 S/cm at room temperature for the p- and n-type respectively. As a result, the fabrication of this metal-free flexible module based solely on these TE materials, leads to the realization of a powerful OTEG device with superior TE performance.

We believe that the methodology and the architecture proposed in this study for fabrication of a flexible, all-carbon fully printed TEG, improves the filling factor and the power output of the device, makes the metallic interconnections between the p-/n- thermoelements redundant and therefore, shows great potential for the future of flexible or even wearable power-conversion TEGs.
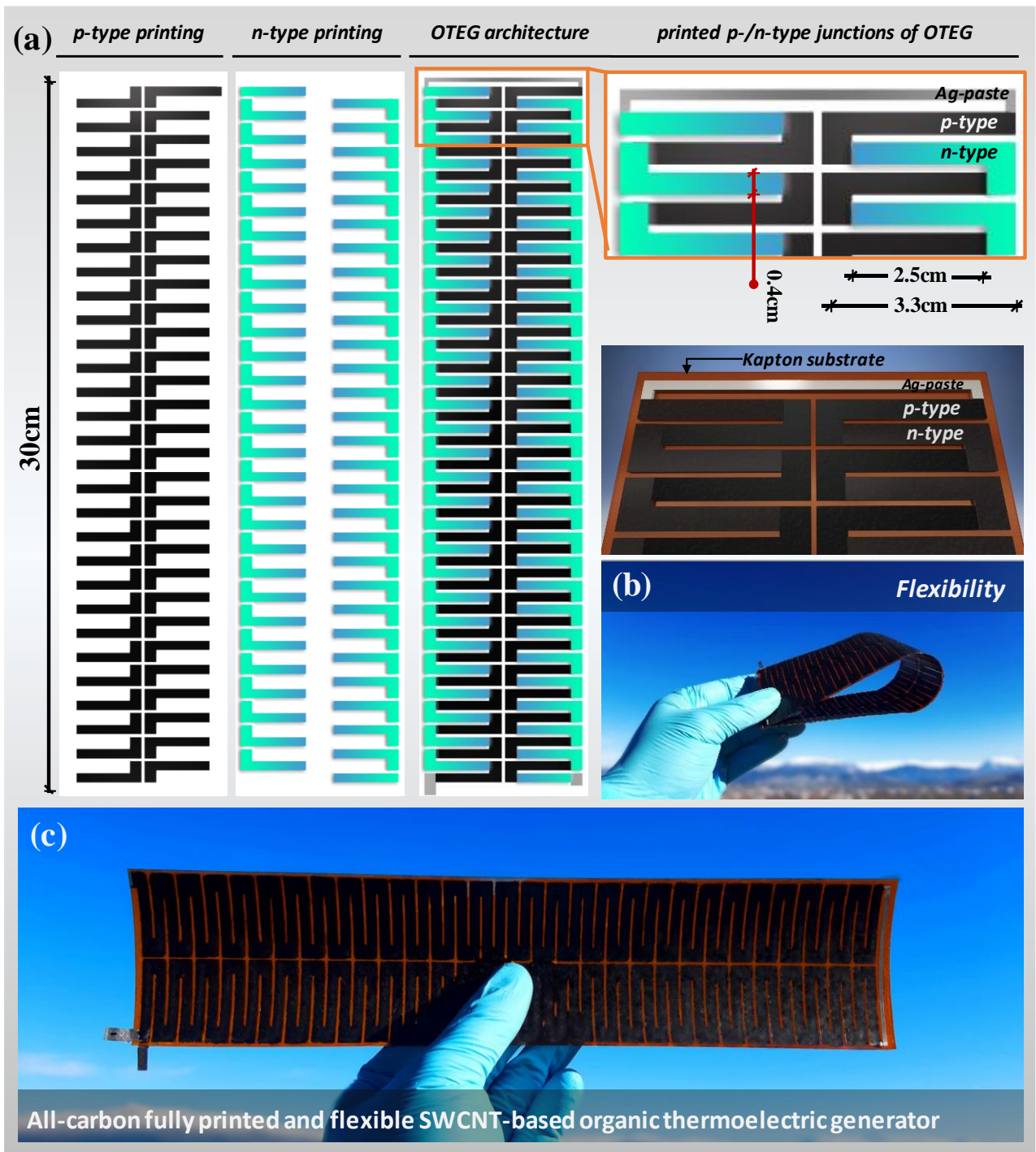
Figure 2. All-carbon fully printed and flexible thermoelectric generator fabrication. (a) Mask assisted device fabrication process via ink dispensing/ printing method onto flexible and high-temperature heat resistant Kapton thin film, (b) the flexibility of OTEG device (c) all-carbon fully printed SWCNT-based OTEG.

4. RESULTS AND DISCUSSION

4.1. Thermoelectric properties, characterisation and stability

In order to manufacture optimal p- and n-type TE inks, various mass ratios of SWCNT:surfactant were added into DI water as dispersion medium. Figure 3 illustrates the thermoelectric properties and characterisation of the produced TE materials. Specifically, Figure 3a-b shows the measured electrical conductivities, Seebeck coefficients as well as the calculated power factors of the p- and n-type SWCNT thin films respectively at different mass ratios. As is mentioned in relevant section for the preparation of TE ink, very low amounts of SDBS do not contribute to good dispersion of CNTs, and resulting in a low-quality TE ink, which is not capable of producing continuous films with high conductivity. As is observed 10:10 and 10:14 mg/mg mass ratios exhibit the highest power factors for p- and n-type TE materials respectively with the specific dimensions of 25mm × 4mm × 5μm. The TE films were manufactured by blade-coating of the semiconducting ink onto a masked Kapton substrate and dried to 90 °C for 20 min as aforementioned in the previous section. When the SWCNTs:CTAB mass ratio increases above 10:14, a decrease in conductivity is observed as the more dielectric CTAB molecules interfere among the conductive SWCNTs without contributing significantly to the Seebeck coefficient. Apart from being high-quality and homogeneous dispersions, the selected TE inks with the higher power factors (PF), also exhibiting a very satisfactory functional viscosity of ~350 cP. As a result, they may also be employed for large-scale printing techniques, (gravure, slot-die, or flexographic printing)[58-60] as shown in Figure 3c.

The long-term stability of the n-type film also studied. Measurements of the electrical conductivity and Seebeck coefficient of the as-prepared n-type SWCNT film without any encapsulation over a period that exceeded 100 days (3.5 months) were performed as shown in Figure 3d. The tests were

carried out in plain air standard environmental conditions (1 atm, ~25 °C, relative humidity: 50±5% RH). During the test period, negligible variations in electrical conductivity and Seebeck coefficient of 3% were observed, proving that the fabricated n-type SWCNTs:CTAB films exhibit outstanding long-term stability in air. This excellent behavior is attributed to the high-quality dispersion which also leads to the creation of surrounding micelles on SWCNTs formed by the small CTAB molecules. Simultaneously, due to the anion-induced electron transfer between the bromide anions (Br⁻) of CTAB on CNTs efficient doping takes place and as a result, both efficient and air-stable n-type TE material is formed. The positive Seebeck coefficient of p-type SWCNT films is mainly a result from oxygen doping in air, which results to hole carriers [39, 62].

As referred in previous works [63-65], nitric acid treatment is often employed for p-doping enhancement. In this study, this method was not preferred as the primary goal was to produce non-toxic TE inks for large-scale and facile printed applications. Nonetheless, the obtained PFs are as high as 240 $\mu W \cdot m^{-1} K^{-2}$ and 210 $\mu W \cdot m^{-1} K^{-2}$ for p- and n-type respectively, and are among the highest values ever reported for non-toxic, flexible and printed organic TE materials [21, 26-29, 31, 56, 66, 67]. The ultrahigh PF can be attributed to the extraordinary electrical conductivities of 2030 $S \cdot cm^{-1}$ and 1432 $S \cdot cm^{-1}$ combined with the reasonably high Seebeck coefficients of 35 $\mu V \cdot K^{-1}$ and -38 $\mu V \cdot K^{-1}$ of p- and n-type films respectively.
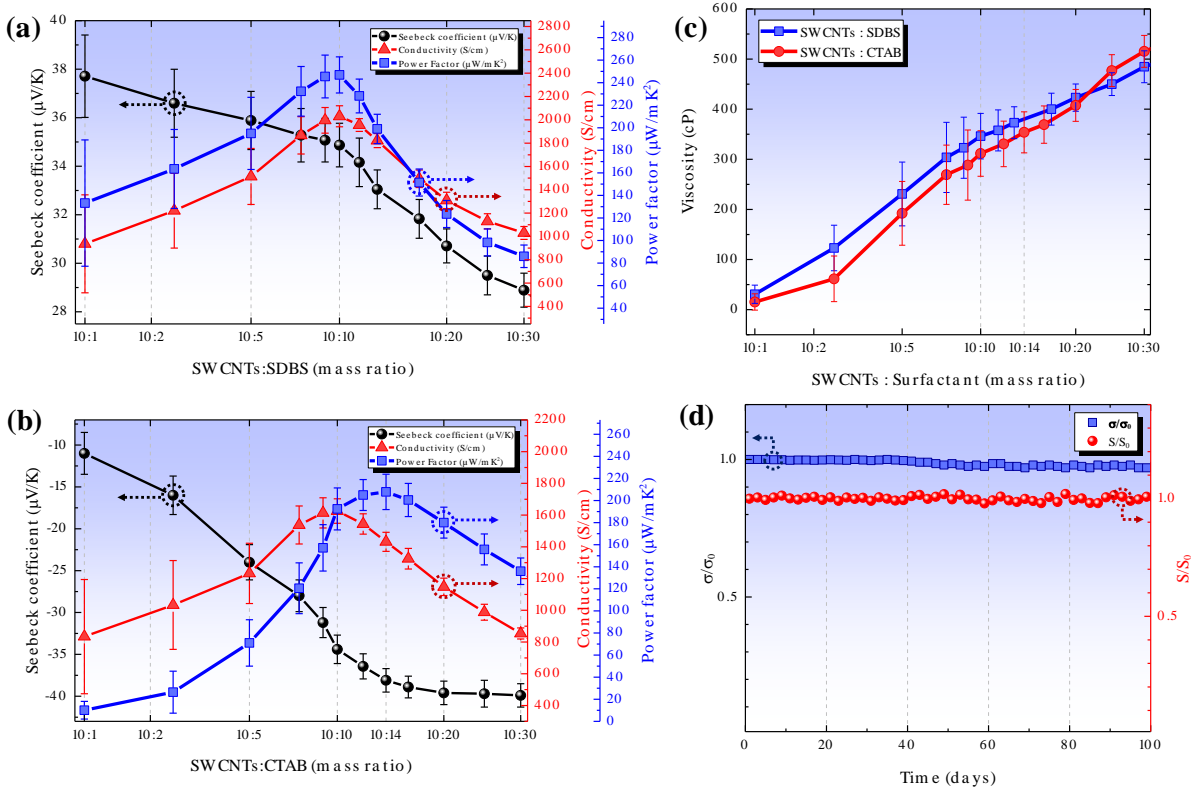
Figure 3. Thermoelectric properties and characterisation of TE materials. (a-b) The measured electrical conductivities, Seebeck coefficients, and the calculated power factors of the p- and n-type SWCNT films respectively at different mass ratios, (c) viscosities of p- and n-type SWCNT TE inks at room temperature and (d) the long-term stability of the flexible n-type SWCNTs:CTAB 10:14 mg/mg film in air without encapsulation.

4.2. *Raman and TGA of p- and n-type SWCNT thermoelements*

Normalized Raman spectra relative to the main graphitic G' band at ca. 1590 cm^{-1} excited with a 514 nm laser for both p-type SWCNTs:SDBS 10:10 mg/mg and n-type SWCNTs:CTAB 10:14 mg/mg TE films shown in Figure 4a. The D band (at ~1,350 cm^{-1}) shows a low intensity compared to the G band (at ~1,590 cm^{-1}) of the Raman spectrum of p-type SWCNT film. This indicates large crystal size and low defects [68]. Compared to the p-type, the n-type thermoelectric film, exhibits similar relative intensities for both D band (at ~1,250 cm^{-1}) and 2D band (at ~2,600 cm^{-1}). This ascertains that no structural defect has been inflicted upon the doping process.

Furthermore, the radial breathing mode (RBM), with a resonance frequency lower than 500 cm^{-1}, represents a bond-stretching out-of-plane phonon mode where all the carbon atoms move cohesively in the radial direction. Similarly, the RBM zone of the n-type film has almost the same intensity with the one of the p-type film, indicating no significant impediment to carbon atom oscillations in the radial direction, such as commonly referred to the PEI doping of SWCNTs [66], also manifested by the high electrical conductivity of CTAB doped structure.

To further examine the doping effect as well as the charge transfer resulting from the CTAB doping, the absorption spectra of the p- and n-type SWCNT films were measured. Figure 4b illustrates the absorption peaks S_{11}, S_{22} and M_{11} of SWCNT films, which can be attributed to the electron transitions between semiconducting and metallic SWCNTs [69]. When the SWCNTs are n-doped with CTAB, the intensities of the semiconducting optical transitions S_{11} and S_{22} display a substantial decrease. This interaction confirms the efficient doping-induced Fermi level deviation, which is consistent with previous studies [54]. When the CTAB mass ratio increases, S_{11} and S_{22} transition attenuations become more noticeable. Absorbance attenuation represents the state-filling of holes or electrons [63, 70]. In combination with the negative Seebeck coefficient of the doped SWCNT films, it is clearly demonstrated that CTAB acts as a very effective n-dopant for CNTs. Furthermore, in order to have a clearer comparison the optical admittance spectroscopy of absorption vs energy of the CNT films is shown in Supplementary Figure 3.

Moreover, thermogravimetric analysis (TGA) was conducted on p- and n-type SWCNT thermoelectric films, in order to assess their thermal performance and limitations, especially for CTAB-doped n-type material, as well as their stability over time at their functional temperature limit. This thermal analysis illustrates the capability and stability of both p- and n-type SWCNT-based organic thermoelectric materials for high temperature applications. Figure 4c shows the p-

type thermal degradation. Zone "I", is attributed to the evaporation of water within the material (0-185°C), zone "II" depicts the onset of SDBS molecules burning (185-450°C), and zone "III" shows the starting point of SWCNT oxidation as well as the burning of the remaining SDBS molecules (450-1000°C). This is consistent with the TGA of SWCNT powder and SDBS powder as shown in Supplementary Figure 4. Figure 4d illustrates the n-type TE material thermal degradation. Zone "I", is attributed to the evaporation of water within the material (0-202°C), zone "II" depicts the sharp burning of most CTAB molecules above the limitation temperature (202-293°C) resulting in an abrupt material degradation and zone "III" shows the burning of the remaining CTAB molecules (293-460°C). Zone "IV" illustrates the starting point of SWCNT oxidation as well as the burning of any remaining molecules (460-1000°C). Concluding, the CTAB-based n-type CNT material, exhibits a stable but sharp high-temperature limit at 200°C, making it suitable for high-temperature applications, which is consistent with previous studies [71, 72]. Approximately 13% of the remaining mass on SWCNTs:CTAB TGA sample is attributed to metal impurities introduced during the SWCNT manufacturing process. The largest percentage of the SWCNTs:SDBS TGA sample is due to the remaining sodium hydrogen sulphite ($NaHSO_3$) molecules, which constitutes the head of the SDBS surfactant [73].
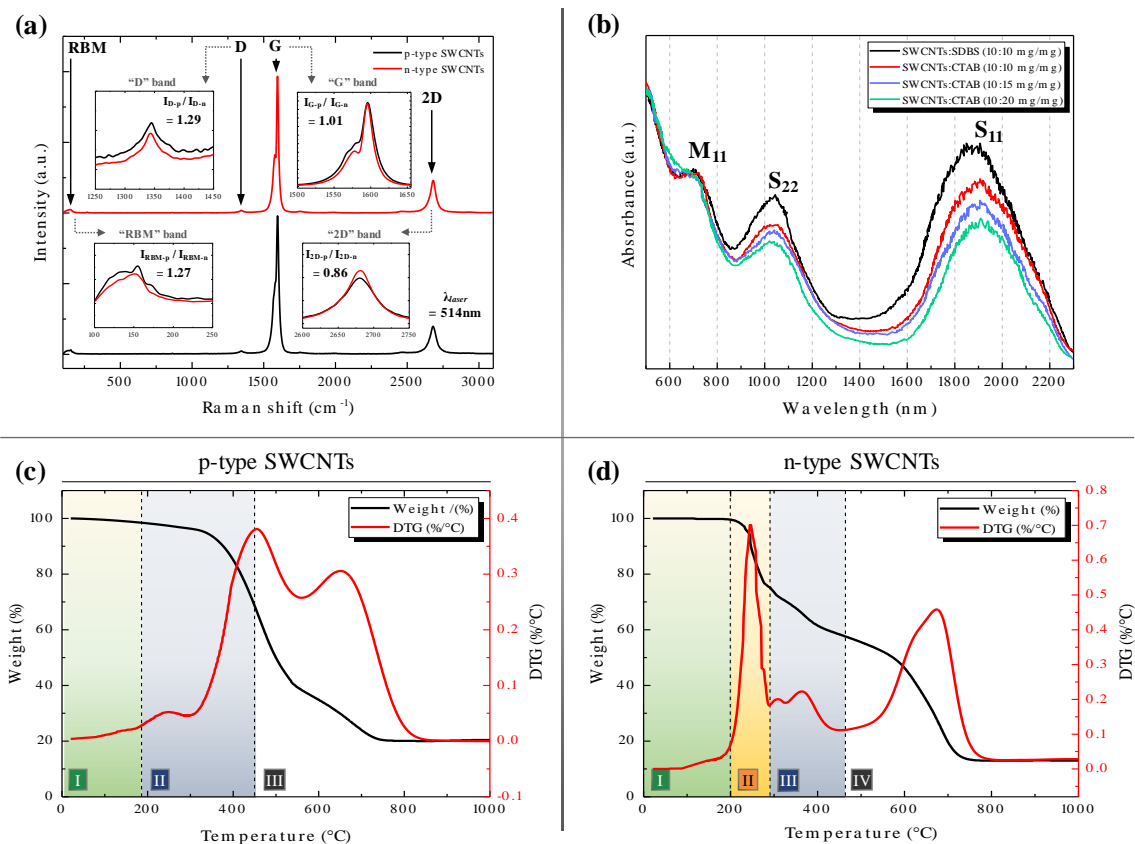
Figure 4. (a) Raman measurements of p- and n-type SWCNTs ,(b) the normalized absorption spectra of the p- and n-type SWCNT films and (c-d) thermogravimetric analysis (TGA) of p- and n-type SWCNT-based semiconducting thermoelements respectively.

4.3. SEM and AFM micrographs

The dispersion quality and the solid-state morphology of the p- and n-doped SWCNT films was compared. Figure 5 shows the focused ion beam-scanning electron microscopy (FIBSEM) as well as the atomic force microscopy (AFM) images of the surfaces of the SWCNT dispersions with anionic and cationic surfactant. As aforementioned, the dispersions were prepared in H_2O, blade-coated at 2.5mm wet film thickness and finally dried at 90°C for 20 min to form in thin films. The well-dispersed p- and n-doped SWCNTs, exhibit similar closely-packed network structures, which contribute effectively to carrier transports. The p-type film network, exhibits excellent continuity

and uniformity (Figure 5a-c). In the n-type SWCNT film (Figure 5d-f), a good dispersion of CNTs with the cationic surfactant is shown, indicating that sufficient CTAB micelles have been formed on CNT surfaces providing an efficient n-type doping due to the anion-induced electron transfer between the bromide anions (Br$^-$) of CTAB on CNTs. In Figure 5d-f, the state of the CTAB dispersion and the coating behaviour for the CTAB-doped SWCNTs is shown. The dispersibility of SWCNTs with CTAB in H$_2$O is also reported in a previous study [57].

The AFM images depict the morphological properties of the respective samples. Figure 5f and Figure 5c illustrate a homogeneous surface coating with a quite low average roughness (Ra) of the examined film after printing the ink, indicating that it has been preceded by a good dispersion. The visible dot spots are indicative of the metal catalyst impurities of the SWCNT material.

As shown in the SEM images (Figure 5b,e), the SWCNT ribbons formed during the drying process of the TE inks, provide a characteristic reticular structure with extraordinary conductivity, which is due to the long Y-type interbundle and intertube junction. As a result, the electrical conductivities of p- and n-type films are 1965 S·cm^{-1} and 1351 S·cm^{-1} respectively at room temperature, which is much higher than reported in previous studies based on polyethyleneimine (PEI) dispersions of CNTs for n-type TE films ($2\times10^3 - 4\times10^4$ S·m^{-1}; refs [27-29, 53]). As is well known, the intertube junctions dominate the electrical conductivity of the SWCNT films. It can therefore be postulated that the much smaller molecules of CTAB provide improved interconnections between the CNTs when compared with PEI and, as a result, much higher electrical conductivity of the TE film is achieved. In conclusion the larger the insulating molecule of the dopant, the less conductive the contacts of the intertube junctions, as carrier transport across the junctions between CNTs is impeded and the electrical conductivity is significantly reduced [74].
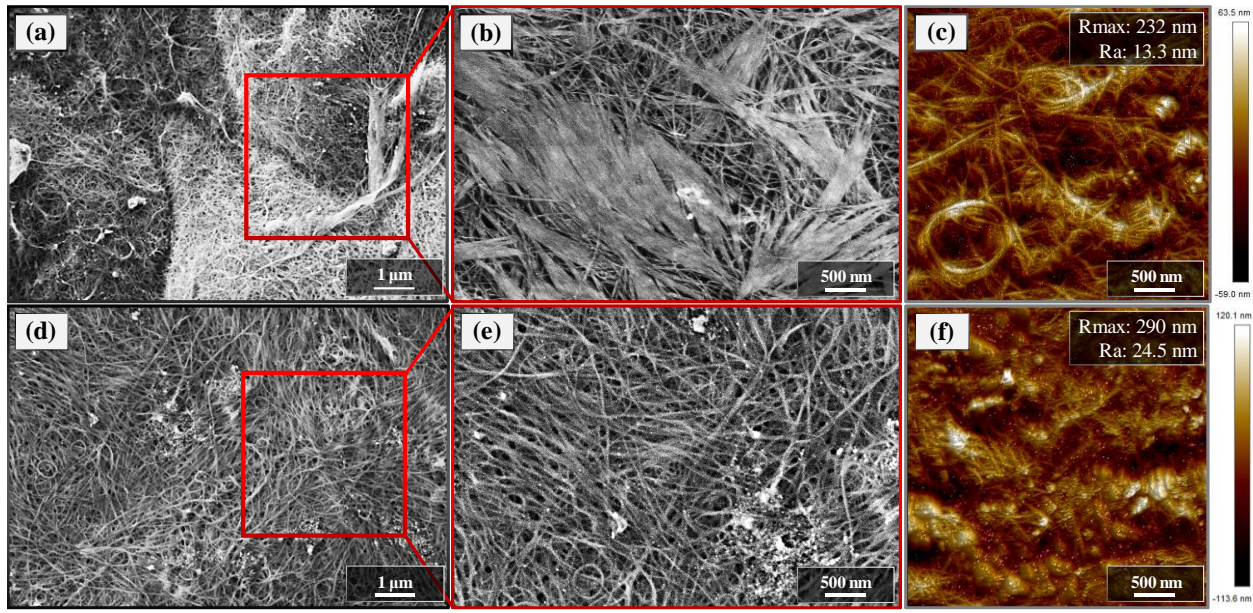
Figure 5. SEM and AFM images of p- and n-type SWCNT printed films, (a,b,c): p-type SWCNTs:SDBS 10:10 mg/mg, (d,e,f): n-type SWCNTs:CTAB 10:14 mg/mg.

4.4. Thermal stability of p- and n-type SWCNT thermoelements

To further investigate the TE behavior of the CNT materials under extreme temperature conditions, a long-term thermal stability based on the TGA was conducted. This was performed, in order to assess the performance of the p- and n-type thermoelements and the capability of high-temperature applications. The tests were performed in an air environment without encapsulation (1 atm, $T_C \simeq 25°C$, relative humidity: $50 \pm 5\%$ RH). Figure 6a-b illustrates the thermal stability and thermoelectric performance of voltage and current of the p-type thermoelement over time. A remarkably stable behavior for both TE characteristics is observed. More analytically, at $\Delta T=100K$ and 125°C set point ($T_C=25°C$, $T_H=125°C$), it took the heat source 149s to gradually reach the required temperature, and the p-type thermoelement 185s to reach its maximum generated thermovoltage , when having the same starting point and time with the heat source. The maximum generated current of the p-type thermoelement, was reached after 211s. Both current and voltage remained perfectly stable for the entire 8-hour testing period. As it is also referred in a previous

study [75], the time lag between the peak of the maximum current and the maximum generated voltage, can be attributed to moisture absorption by the SDBS molecules, indicating that the current is much more sensitive to environmental conditions than voltage. Experiments have shown that the time-averaged current is affected by the relative humidity (RH). More specifically, the apparent mobility of charge carriers decreases as relative humidity increases because the additional mass of ions reduces their mobility. As the temperature rises and the water absorbed molecules evaporate, the resistance of the material decreases, thereby the generated current increases [75, 76]. Figure 6c-d depicts the thermal stability and thermoelectric performance of voltage and current of the n-type thermoelement as a function of time. Again, both TE characteristics are remarkably stable. For the experimental conditions at $\Delta T=100K$ ($T_C=25°C$, $T_H=125°C$) the maximum generated voltage was reached after 187s, the maximum generated current after 643s and remained stable for the entire 8-hour testing period. This difference between the peak-time of the generated current and voltage reveals that CTAB molecules are much more sensitive to moisture absorption than SDBS and therefore a stronger diversification in the measured peak times is observed [75, 76].

Figure 6e-f illustrates the temperature dependency and degradation of the n-type dopant of the thermoelement after exposure to marginally extreme temperatures as a function of time. It is demonstrated that after being exposed to 220°C, the n-type material begins to degrade in terms of voltage and current after ca. 20 min. Full degradation takes place after ca. 3 hours, when the dopant is completely eliminated. It may be therefore concluded that CTAB apart from being a very good n-type doping agent, also maintains its n-type character. This is attributed to the very efficient bonding with the CNTs and the remarkable high-temperature stability in air. At the same time high quality aqueous dispersions of SWCNT with CTAB are achieved [77] . The TGA study and the thermal stability of the CTAB-based n-type SWCNT thermoelement, prove the stability and the

high-temperature endurance of up to 200°C, which is among the highest value ever reported for organic TE materials [53, 78]. Furthermore, the employed in-plane architecture of thermoelements for the OTEG device fabrication proves to be very stable for all studied ΔT as a function of time. Conversely, the short thermoelements of the conventional through-thickness TEG geometries, are reported to suffer from a rapid increase of T_C temperature close to T_H as thermal equilibrium is rapidly reached, resulting in the decrease of ΔT, and inevitably an attenuated power output [79].
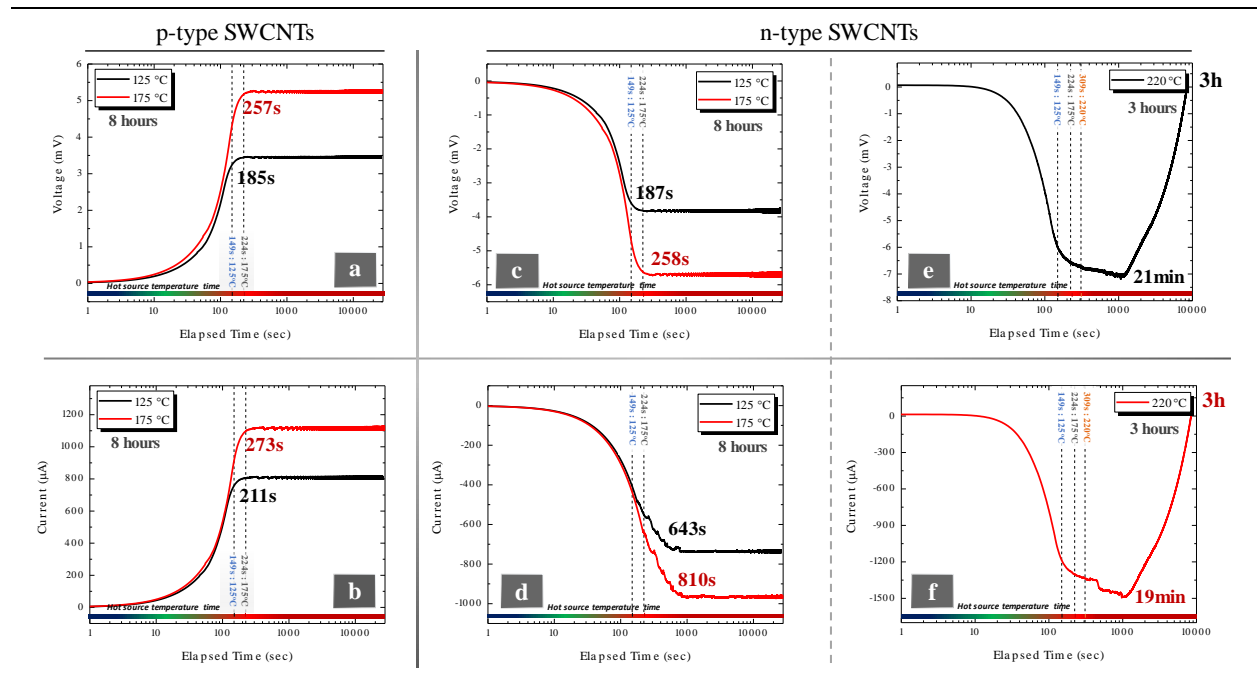

Figure 6. Thermal stability and performance of (a-b) p-type, (c-d) n-type TE materials at 125°C and 175°C. (e-f) The temperature dependency and the degradation of the n-type dopant after exposure to extreme temperatures as a function of time.

4.5. *Thermoelectric characterisation of p- and n-type SWCNT thermoelements*

The TE properties of SWCNT-based materials where thoroughly studied in terms of their thermoelectric behavior. More analytically, the Seebeck coefficient, electrical conductivity, thermal conductivity, power factor, figure of merit and the thermoelectric efficiency of the TE

materials as a function of temperature were measured or calculated. The maximum efficiency of a thermoelectric material can be determined by its thermoelectric figure of merit (zT). given by [80]:

$$zT = \frac{\sigma S^2 T}{\kappa} \qquad (1)$$

where S is the Seebeck coefficient, σ the electrical conductivity, κ the thermal conductivity, and T the absolute temperature. The optimal efficiency of thermal to electrical energy conversion for a thermoelectric material is expressed as [81, 82]:

$$\eta = \left(\frac{T_H - T_C}{T_H}\right)\frac{\sqrt{1 + Z\overline{T}} - 1}{\sqrt{1 + Z\overline{T}} + (T_C/T_H)} \qquad (2)$$

The first factor in (2) is the Carnot efficiency. The second factor which is a function of $Z\overline{T}$, determines what fraction of the Carnot efficiency can be obtained from a TEG under a given ΔT. T_H represents the temperature at the hot junction and T_C is usually a steady temperature of a surface that remains cold. The temperatures at the hot side (T_H) and the cold side (T_C) of a TE material define the temperature difference ($T_H - T_C$), and $\overline{T}$ is the average of these temperatures.

Figure 7a,b illustrates the thermoelectric performance of p-type SWCNTs:SDBS 10:10 mg/mg and n-type SWCNTs:CTAB 10:14 mg/mg TE materials as a function of temperature. The thermoelectric material characterization measurements were performed using the Linseis-TFA instrument. TFA has an integrated microchip, where the thermal conductivity and Seebeck measurement are performed using a hotwire setup located on a suspended membrane setup. The membrane part (T_H) can be heated independently from the surrounding chip, which is kept at room temperature (T_C). The outstanding σ of 2065 S/cm and 1474 S/cm are noteworthy as well as the

notably high S of 38.6 µV/K and -41.8 µV/K at $\Delta T=150K$ ($T_C=25°C$). These result to the significantly enhanced PFs of 308 µW/mK^2 and 258 µW/mK^2 for the printed p- and n-type organic TE materials respectively. The measured κ values for the TE thin films are 0.15 W/mK and 0.12 W/mK for the p- and n-type thin films at room temperature and decrease as the temperature increases, which is consistent with previous studies [83-85].

Finally, the ultrahigh zT of 1.14 and 1.21 at $\Delta T=150K$, provide the extraordinary conversion efficiencies of 6.26% and 6.56% for the p- and n-type TE materials respectively, which is among the highest value ever reported for organic TE materials [31, 86, 87]. It is also worth noting the remarkable power factors of 145 µW/mK^2 and 127 µW/mK^2 for the p-type and n-type films respectively at room temperature. As these values result from low-cost, non-toxic, abundant, flexible and facile to manufacture TE materials, the future of organic thermoelectrics proves to be promising.
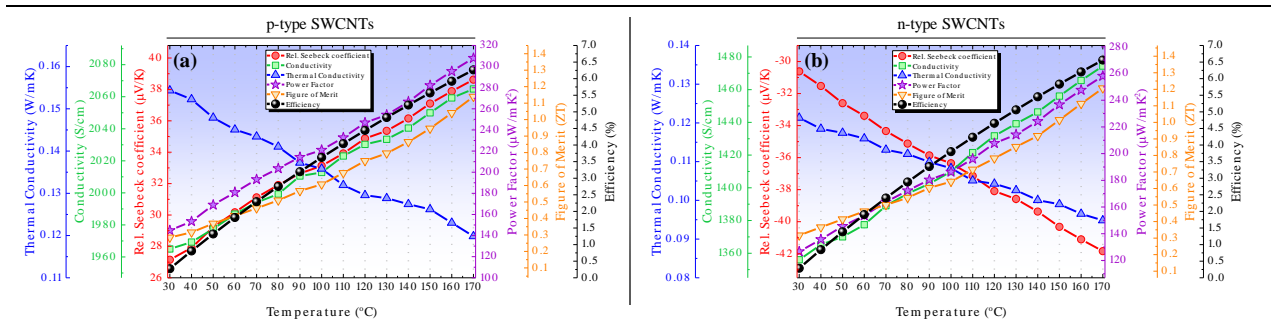

Figure 7. Thermoelectric performance of (a) p-type and (b) n-type TE materials as a function of temperature.

4.6. Performance and demonstration of OTEG device

The fabricated OTEG device exhibits an outstanding performance, which is due to the excellent TE properties of the p- and n-type printed and flexible thin films using the well dispersed SWCNT inks. When the fabricated OTEG is exposed to a temperature difference (ΔT) between the center

and both sides of the module in the in-plane direction, a significant voltage is generated due to the Seebeck effect. Figure 8 illustrates the measured thermoelectric performance of the OTEG device in various steady ΔT. All tests were performed in ambient conditions without encapsulation (1 atm, $T_C \simeq 25°C$, relative humidity: $50 \pm 5\%$ RH). The printed and flexible OTEG module with dimensions of 30 cm $\times$ 7 cm $\times$ 110 μm, exhibits a thermopower of 7791 μV/K at $\Delta T = 100$K ($T_H = 125°C$), which is 92% consistent with the theoretically calculated values of 8468 μV/K. A should be noted, the novel OTEG device architecture shows excellent TE performance for each thermoelement, without the need for metallic interconnections. This is mainly due to the high conductivity of the SWCNTs, as well as the short interconnection distance between the thermoelements. As aforementioned, the contact resistance between the metal electrode and the CNTs is higher than the resistance of the metal or the CNT itself, resulting in reduced power output [61], which is not the case in the proposed OTEG, where highly conductive SWCNTs are solely employed.

The open-circuit voltage $V_{OC} = 1.05$ V and short-circuit current $I_{SC} = 1.30$ mA were achieved at $\Delta T = 150$ K ($T_H = 175°C$) with an internal resistance $R_{TEG} = 806$ Ω. This resulted to the ultra-high power output of 342 μW, as shown in Figure 8 and Figure 9. The power density of the OTEG can be determined by the following equation [88].

$$P_{density} = \frac{P_{max}}{N \cdot A} = \frac{(N \cdot S \cdot \Delta T)^2/4 \cdot N \cdot \frac{l}{\sigma \cdot w \cdot d}}{N \cdot w \cdot d} = \frac{S^2 \cdot \sigma}{4l} \cdot \Delta T^2 \tag{3}$$

where N is the number of the thermoelement, A represents the area of the thermoelement, w, d, and l are the width, thickness, and length of the thermoelements respectively. The achieved maximum power density of the OTEG device is 1.79 W/m^2 and 7.38 W/m^2 at $\Delta T = 50$K and

ΔT=150K respectively (T$_C$=25°C). The specific power (estimated by dividing the measured P$_{max}$ by the total mass of the module) is 0.65 mW/g and 3.69 mW/g at ΔT=50K and ΔT=150K respectively, which is among the highest values ever reported for printed organic thermoelectric generators [10, 24, 28, 31, 41, 57, 66 88-94]. Supplementary Figure 5 illustrates a comparison between the power factors of our printed p- and n-type organic TE materials as well as the power density between our flexible OTEG device with the reported ones.

Figure 9 depicts the OTEGs' performance at ΔT=150K as well as potential applications for the fabricated OTEG module on a human arm and on a heated tube of a working radiator. When the human arm is in touch with the central active stripe of the OTEG, while the side-ends of the module are insulated with styrofoam, a large Seebeck voltage of 71 mV is rapidly observed (Figure 9c-d) at room temperature (T$_C$~25°C). During the wearable application of the OTEG, a short-circuit current of 119 μA and a power output of 2.1 μW was achieved at ΔT=6 K, a temperature difference that can be easily achieved between a human body and the external environment as also have been reported in previous studies [61, 93-96].
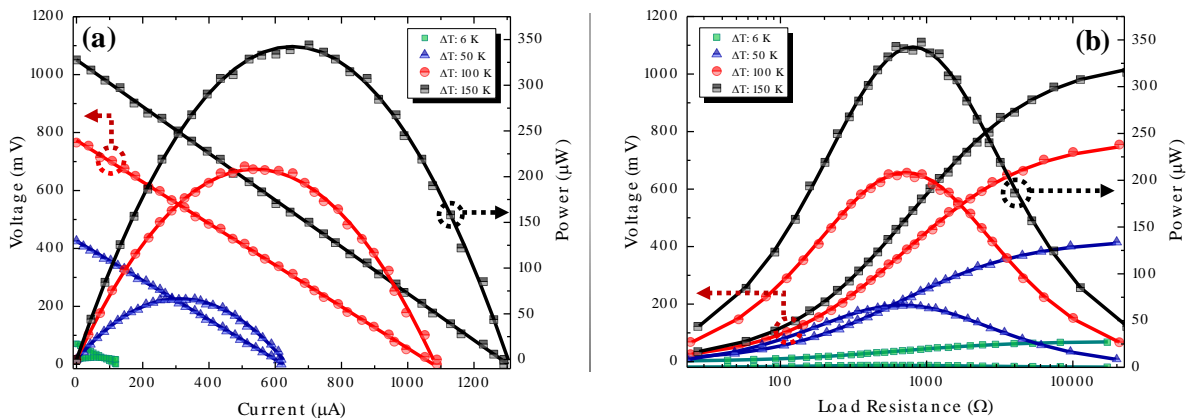

Figure 8. Thermoelectric performance of OTEG in various ΔT. (a) Voltage-Current (V-I), Power-Current (P-I) curves and (b) Voltage-Load resistance (V-R$_{LOAD}$), Power-Load resistance (P-R$_{LOAD}$) curves.
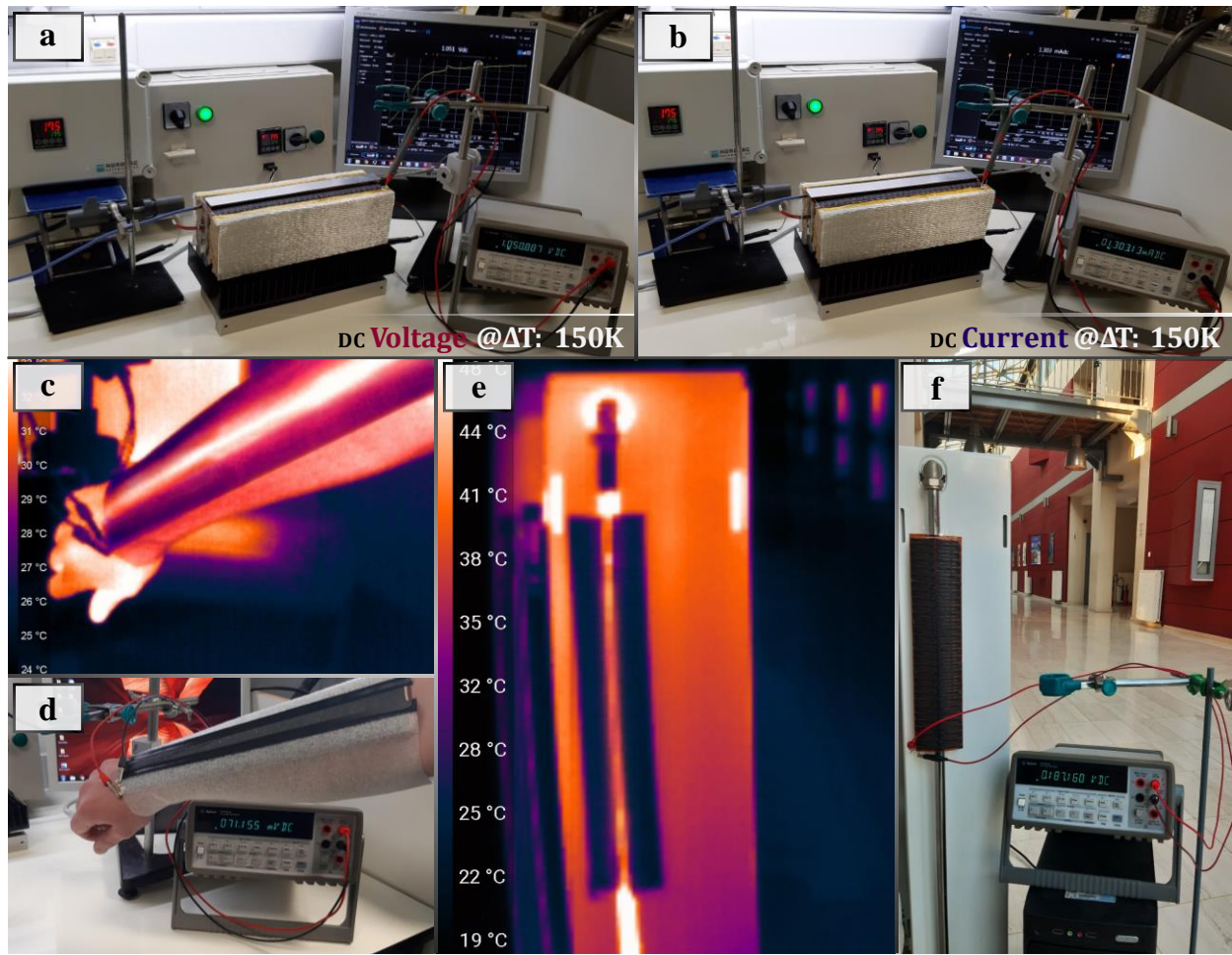
Figure 9. OTEG-device performance at (a-b) ΔT:150K. Application of OTEG-device at (c-d) a human arm and (e-f) at a heated tube of a working radiator.

It is therefore demonstrated that the manufactured OTEG can be an effective device for harvesting biothermal power, thus giving great potential for energy-harvesting wearables as shown in Figure 8 and Figure 9c-d. As will be further demonstrated, the very good flexibility of the OTEG facilitates its use for these applications. A more detailed description of the thermoelectric performance and the wearable design of the OTEG can be found in Supplementary Figures 5 and 6 respectively. As aforementioned, the OTEG was also placed around the hot tube of a working radiator. Typically, the inlet water temperature for a working radiator is ca. 75°C. For a room temperature ca. 25°C, the OTEG has achieved a stable power output of 66 μW at ΔT=50K. Both

simple experiments indicate that common waste heat in the ambient environment can efficiently be converted to electric energy by using our flexible OTEG device.

In addition to the previous study, the OTEG was employed to charge a commercial step-up converter (Advanced Linear Devices- EH4295) and power up a green LED. ALD-EH4295 step-up converter has a fixed internal voltage of 1.6V and must be increased to 3.8V to be able to power-up an electronic component. In order to start charging the ALD-EH4295, the input power must exceed the minimum value of 2 μW. The OTEG device can generate 2.1 μW at ΔT=6K which is the case in contact with the human body surpassing the minimum 2 μW power requirement for the initiation of the charging of the EH4295. Under these conditions it was possible to power up the green LED after 3478 seconds (~58 minutes) of charging. Figure 10 depicts the time required of the OTEG to charge the commercial EH4295 step-up converter in various temperatures. For ΔT=50K and ΔT=150K, charging times of 208 sec and 48 sec respectively are achieved to step-up the voltage from 1.6V to 3.8V and power up a green LED. Figure 11 illustrates the experimental setup and the electronic board with the EH4295 step-up converter used to power up a green LED at ΔT=100K and in contact with the human body (at ΔT=6).
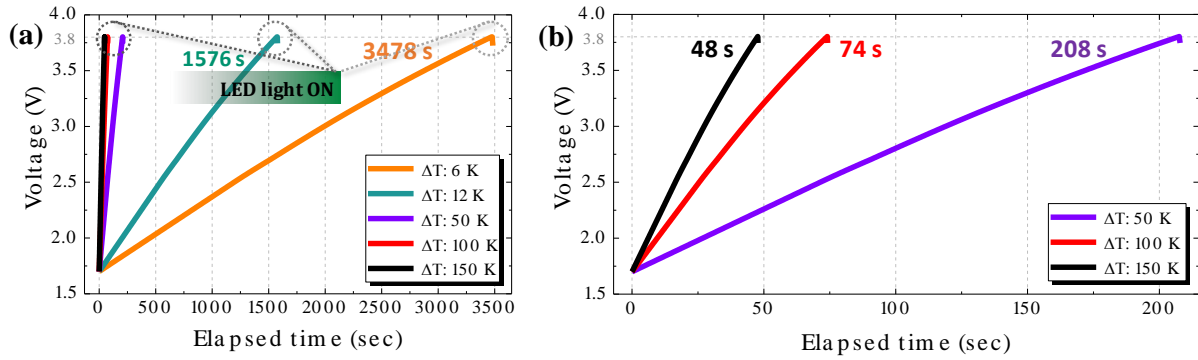
Figure 10. The elapsed time required to charge a commercial step-up converter (ALD-EH4295) using the generated power form the OTEG device in order to power a green LED (a) at four different temperatures and (b) at three different temperatures.
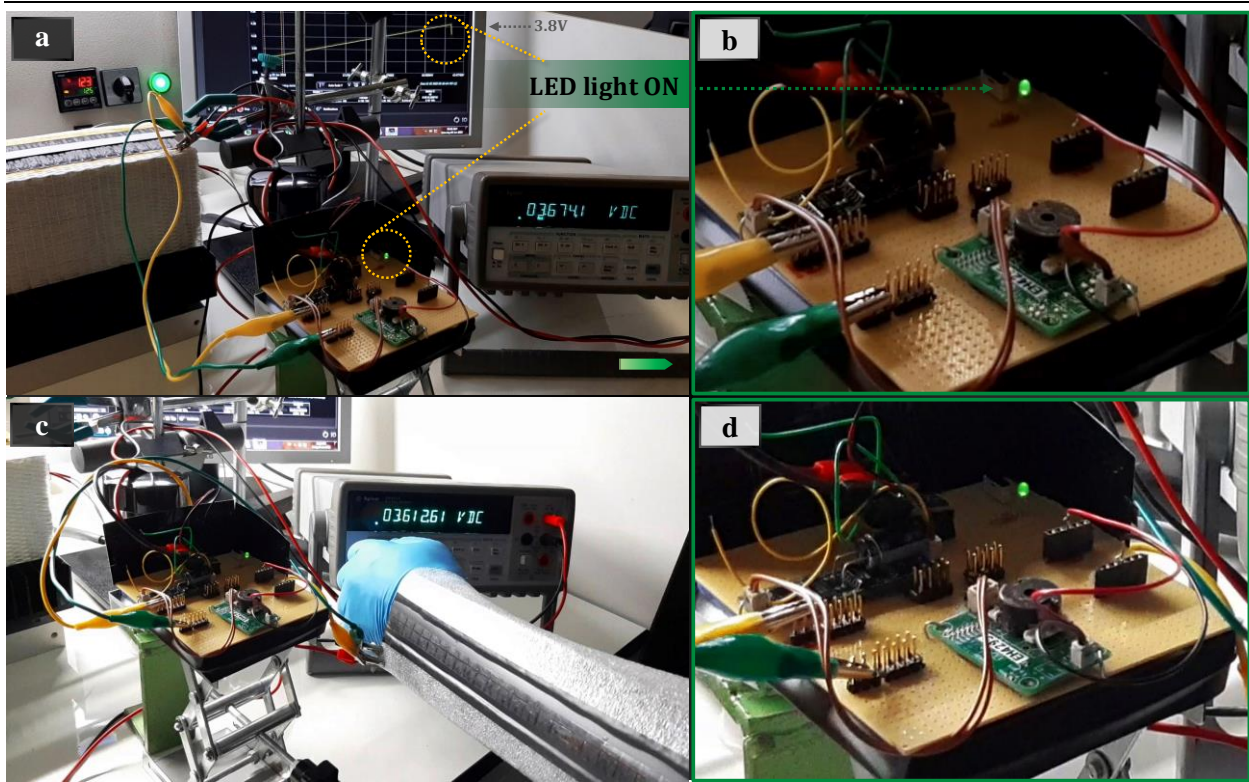

Figure 11. The experimental setup and the electronic board with the EH4295 step-up converted used to power up a green LED (a-b) at $\Delta T=100K$ and (c-d) in contact with the human body.

4.7. Flexibility tests of the OTEG device

In recent studies, various TEG devices based on organic TE materials are fabricated [17, 27, 28, 51, 53, 97, 98]. However, they demonstrate low performance due the relatively low PFs of the constituent TE materials. Inspired by our research results described above, we fabricate a novel-configuration of all-carbon fully printed, highly flexible and efficient TEG module based on non-toxic SWCNT aqueous dispersions.

A quantitative measurement of the bending radius of the fabricated module was conducted by rolling the OTEG device onto a round object. The flexibility of TEG device is essential so that the active area comes in close contact with the heated surface. This is indispensable for heat sources with irregular surfaces in order to take advantage of ubiquitous waste heat. A conventional TE module with a π shaped configuration consists of p- and n-type TE materials, which are electrically connected in series by metallic interconnections. In addition, dozens of gold or silver nanometers are usually deposited as top electrodes on each thermoelement in order to decrease the contact resistance. Compared with a conventional TEG, our module does not contain brittle metallic interconnections between p- and n-type thermoelements exhibiting excellent flexibility as shown in Figure 12.

Figure 12a illustrates the resistance change ratios of the fabricated OTEG as a function of bending radius ranging from 5 cm to 1.5 cm in the short (A-A') and long axis (B-B') directions. The resistance change ratio is defined as $\Delta R/R_0$, where R_0 refers to the initial internal resistance of the OTEG module and ΔR refers to the resistance difference between the real-time resistance tested under special operation and R_0 ($\Delta R = R - R_0$). When the OTEG was bent along the A-A' and B-B' axis up to a radius of 1.5 cm, the resistance change ratio of the module was 0.4% and 1.3%

respectively, or else, the total internal resistance change is negligible, as shown in Supplementary Figure 7.

Figure 12b shows the $\Delta R/R_0$ vs the generated voltage after multiple bending repetitions for a radius of 3 cm. After 1000 bending cycles, the $\Delta R/R_0$ of the module were 0.8% and 1.9% at the A-A' and B-B' axis respectively. At the same time and for $\Delta T=150°C$ ($T_H=175°C$), the output voltage of the device remained almost constant. In Figure 12c the $\Delta R/R_0$ vs the increase of the temperature of the module is depicted. As can be observed, it exhibits an almost linear behavior with an average increase of 2.5% per 10°C. Finally, as shown in Figure 12d, the endurance of the OTEG was studied over 100 heating cycles, where the internal resistance of the module as well as the generated voltage of device remained remarkably constant. Concluding, it is demonstrated that the developed OTEG module possesses remarkable flexibility, stability and endurance, which renders it a highly reliable organic thermoelectric generator capable for both energy-harvesting wearables as well as for high-temperature applications up to 200°C.
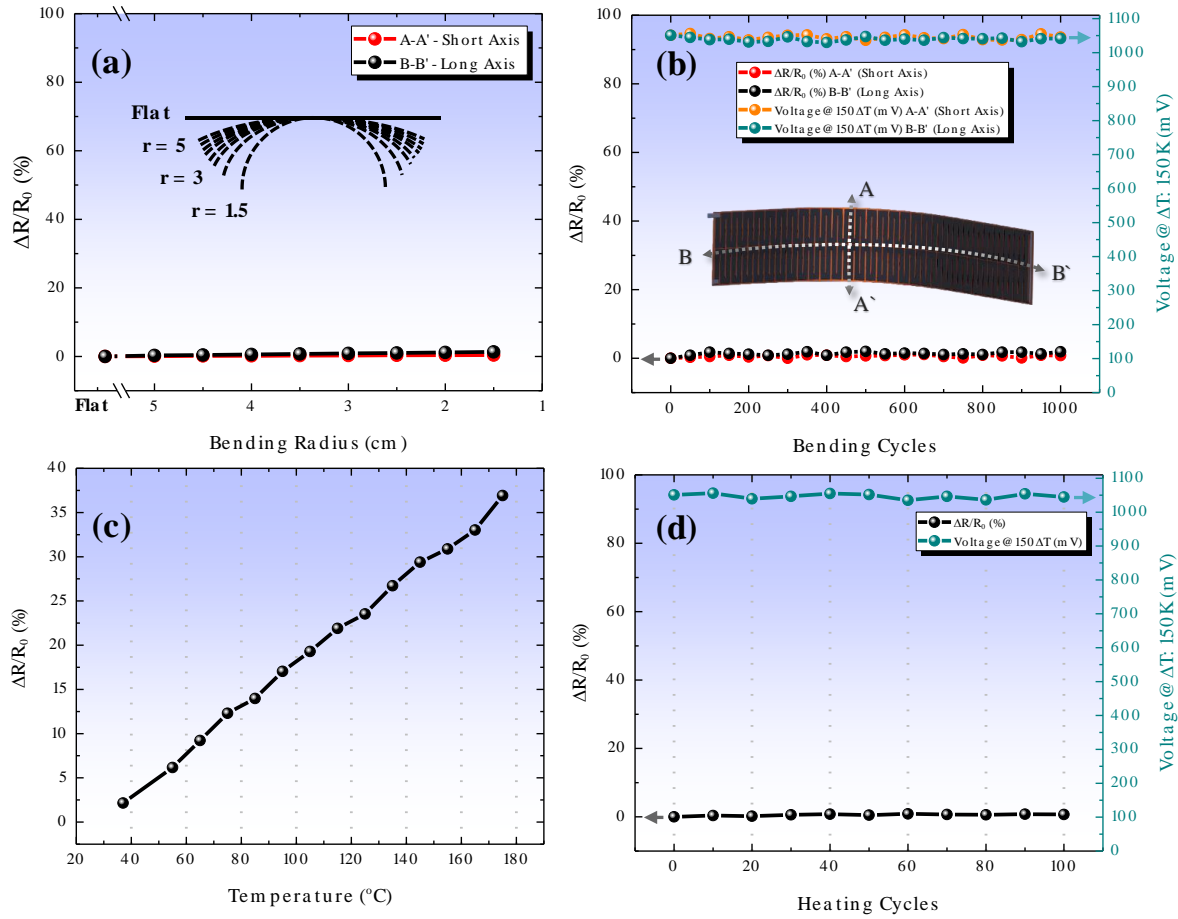
Figure 12. Flexibility and reliability tests of the developed OTEG device. (a) Resistance change ratios ($\Delta R/R_0$) of the OTEG in bending state with various radii. (b) $\Delta R/R_0$ and generated voltage in different bending cycle at $\Delta T = 150°C$. (c) $\Delta R/R_0$ as a function of temperature. (d) The repeatability of the $\Delta R/R_0$ as well as the generated voltage of the OTEG over 100 heating cycles at $\Delta T = 150°C$.

5. CONCLUSIONS

In this work, we develop non-toxic, facile, low-cost, high-temperature resistant, air-stable and flexible p- and n-type organic TE films based on aqueous SWCNT dispersions. Moreover, we demonstrate a novel-designed fully printed, all-carbon and flexible organic thermoelectric generator (OTEG) with extraordinary TE performance, consisting of p- and n-type thermoelectric thin films. The SWCNT-based TE printed films are also employed for the interconnections

between the p-/n- thermoelements to minimize the circuit resistance due to their superior electrical conductivity, while providing excellent flexibility [61]. The optimum p-type film of SWCNTs:SDBS 10:10 mg/mg and n-type film of SWCNTs:CTAB 10:14 mg/mg, exhibit the remarkable PFs of 308 $\mu W/mK^2$ and 258 $\mu W/mK^2$ respectively at $\Delta T=150$ K ($T_H=175°C$). In addition, a long-term stability in air without encapsulation with negligible loss in electrical conductivity and Seebeck coefficient ($\sim$3% during a 3.5-month test period) was observed. Furthermore, the proposed in-plane architecture of thermoelements, exhibits extraordinary stable overall TE performance for various ΔT as a function of time, conversely to the short thermoelements of conventional through-thickness TEGs, which lead to a rapid increase of T_C close to T_H and an attenuated power output [79]. The novel-design OTEG exhibits an ultra-high open-circuit voltage $V_{OC}=1.05$ V and short-circuit current $I_{SC}=1.30$ mA at $\Delta T=150$K ($T_H=175°C$) with an internal resistance $R_{TEG}=806$ Ω. As a result, the remarkable power output of 342 μW is achieved, which is among the highest values ever reported for printed and flexible organic thermoelectric generators. It is also worth noting the remarkable power factors of 145 $\mu W/mK^2$ and 127 $\mu W/mK^2$ for the p-type and n-type films respectively at room temperature. The reported high efficiencies achieved via non-toxic aqueous TE inks, providing huge potential for printable, roll-to-roll (R2R) or sheet-to-sheet (S2S) large-scale industrial production of organic thermoelectric generators, with a high impact to the renewable energy sources market.

CONFLICTS OF INTEREST

There are no conflicts to declare.

ASSOCIATED CONTENT

Supporting Information.

Supporting Information is available from the Journal website or from the author.

AUTHOR INFORMATION

Corresponding Authors

* E-mail: cmytafides@gmail.com (Christos K. Mytafides)

** E-mail: latzounis@gmail.com (Lazaros Tzounis)

*** E-mail: paipetis@uoi.gr (Alkiviadis S. Paipetis)

ORCID

Christos K. Mytafides: 0000-0003-4560-867X

Lazaros Tzounis: 0000-0003-0567-3020

Alkiviadis S. Paipetis: 0000-0001-9668-9719

Notes

The authors declare no competing financial interest.

ACKNOWLEDGEMENTS

REFERENCES

1.   Forman, C.; Muritala, I. K.; Pardemann, R.; Meyer, B., Estimating the global waste heat potential. *Renewable and Sustainable Energy Reviews* **2016,** *57*, 1568-1579.

2.   Kanatzidis, M. G., Chapter 3 The role of solid-state chemistry in the discovery of new thermoelectric materials. In *Semiconductors and Semimetals*, Tritt, T. M., Ed. Elsevier: 2001; Vol. 69, pp 51-100.

3.   He, M.; Zhao, Y.; Wang, B.; Xi, Q.; Zhou, J.; Liang, Z., 3D Printing Fabrication of Amorphous Thermoelectric Materials with Ultralow Thermal Conductivity. *Small* **2015,** *11* (44), 5889-5894.

4.   Yin, X.; Liu, J.-Y.; Chen, L.; Wu, L.-M., High Thermoelectric Performance of In4Se3-Based Materials and the Influencing Factors. *Accounts of Chemical Research* **2018,** *51* (2), 240-247.

5.   Yusupov, K.; Stumpf, S.; You, S.; Bogach, A.; Martinez, P. M.; Zakhidov, A.; Schubert, U. S.; Khovaylo, V.; Vomiero, A., Flexible Thermoelectric Polymer Composites Based on a Carbon Nanotubes Forest. *Advanced Functional Materials* **2018,** *28* (40), 1801246.

6.   Choi, H.; Kim, Y. J.; Kim, C. S.; Yang, H. M.; Oh, M.-W.; Cho, B. J., Enhancement of reproducibility and reliability in a high-performance flexible thermoelectric generator using screen-printed materials. *Nano Energy* **2018,** *46*, 39-44.

7.   Kim, C. S.; Yang, H. M.; Lee, J.; Lee, G. S.; Choi, H.; Kim, Y. J.; Lim, S. H.; Cho, S. H.; Cho, B. J., Self-Powered Wearable Electrocardiography Using a Wearable Thermoelectric Power Generator. *ACS Energy Letters* **2018,** *3* (3), 501-507.

8.   Yang, L.; Chen, Z.-G.; Dargusch, M. S.; Zou, J., High Performance Thermoelectric Materials: Progress and Their Applications. *Advanced Energy Materials* **2018,** *8* (6), 1701797.

9.   Heremans, J. P.; Dresselhaus, M. S.; Bell, L. E.; Morelli, D. T., When thermoelectrics reached the nanoscale. *Nature Nanotechnology* **2013,** *8*, 471.

10.   Russ, B.; Glaudell, A.; Urban, J. J.; Chabinyc, M. L.; Segalman, R. A., Organic thermoelectric materials for energy harvesting and temperature control. *Nature Reviews Materials* **2016,** *1* (10), 16050.

11.   Chen, G.; Xu, W.; Zhu, D., Recent advances in organic polymer thermoelectric composites. *Journal of Materials Chemistry C* **2017,** *5* (18), 4350-4360.

12.   Hu, X.; Chen, G.; Wang, X.; Wang, H., Tuning thermoelectric performance by nanostructure evolution of a conducting polymer. *Journal of Materials Chemistry A* **2015,** *3* (42), 20896-20902.

13.   Biswas, K.; He, J.; Zhang, Q.; Wang, G.; Uher, C.; Dravid, V. P.; Kanatzidis, M. G., Strained endotaxial nanostructures with high thermoelectric figure of merit. *Nature Chemistry* **2011,** *3* (2), 160-166.

14.   Zhao, W.; Fan, S.; Xiao, N.; Liu, D.; Tay, Y. Y.; Yu, C.; Sim, D.; Hng, H. H.; Zhang, Q.; Boey, F.; Ma, J.; Zhao, X.; Zhang, H.; Yan, Q., Flexible carbon nanotube papers with improved thermoelectric properties. *Energy & Environmental Science* **2012,** *5* (1), 5364-5369.

15.   Nakai, Y.; Honda, K.; Yanagi, K.; Kataura, H.; Kato, T.; Yamamoto, T.; Maniwa, Y., Giant Seebeck coefficient in semiconducting single-wall carbon nanotube film. *Applied Physics Express* **2014,** *7* (2), 025103.

16.   Chen, J.; Gui, X.; Wang, Z.; Li, Z.; Xiang, R.; Wang, K.; Wu, D.; Xia, X.; Zhou, Y.; Wang, Q.; Tang, Z.; Chen, L., Superlow Thermal Conductivity 3D Carbon Nanotube Network for Thermoelectric Applications. *ACS Applied Materials & Interfaces* **2012,** *4* (1), 81-86.

17.   Bubnova, O.; Khan, Z. U.; Malti, A.; Braun, S.; Fahlman, M.; Berggren, M.; Crispin, X., Optimization of the Thermoelectric Figure of Merit in the Conducting Polymer Poly(3,4-ethylenedioxythiophene). *Nat. Mater.* **2011,** *10*, 429.

18.   Park, T.; Park, C.; Kim, B.; Shin, H.; Kim, E., Flexible PEDOT electrodes with large thermoelectric power factors to generate electricity by the touch of fingertips. *Energy & Environmental Science* **2013,** *6* (3), 788-792.

19.   Kim, G. H.; Shao, L.; Zhang, K.; Pipe, K. P., Engineered Doping of Organic Semiconductors for Enhanced Thermoelectric Efficiency. *Nat. Mater.* **2013,** *12*, 719.

20.   Zhang, Q.; Sun, Y.; Xu, W.; Zhu, D., Organic Thermoelectric Materials: Emerging Green Energy Materials Converting Heat to Electricity Directly and Efficiently. *Advanced Materials* **2014,** *26* (40), 6829-6851.

21.   Cho, C.; Stevens, B.; Hsu, J.-H.; Bureau, R.; Hagen, D. A.; Regev, O.; Yu, C.; Grunlan, J. C., Completely Organic Multilayer Thin Film with Thermoelectric Power Factor Rivaling Inorganic Tellurides. *Advanced Materials* **2015,** *27* (19), 2996-3001.

22.   Yu, C.; Choi, K.; Yin, L.; Grunlan, J. C., Light-Weight Flexible Carbon Nanotube Based Organic Composites with Large Thermoelectric Power Factors. *ACS Nano* **2011,** *5* (10), 7885-7892.

23.   Yao, Q.; Chen, L.; Zhang, W.; Liufu, S.; Chen, X., Enhanced Thermoelectric Performance of Single-Walled Carbon Nanotubes/Polyaniline Hybrid Nanocomposites. *ACS Nano* **2010,** *4* (4), 2445-2451.

24.   Kim, D.; Kim, Y.; Choi, K.; Grunlan, J. C.; Yu, C., Improved Thermoelectric Behavior of Nanotube-Filled Polymer Composites with Poly(3,4-ethylenedioxythiophene) Poly(styrenesulfonate). *ACS Nano* **2010,** *4* (1), 513-523.

25.   Yu, C.; Kim, Y. S.; Kim, D.; Grunlan, J. C., Thermoelectric Behavior of Segregated-Network Polymer Nanocomposites. *Nano Letters* **2008,** *8* (12), 4428-4432.

26.   Wang, H.; Hsu, J.-H.; Yi, S.-I.; Kim, S. L.; Choi, K.; Yang, G.; Yu, C., Thermally Driven Large N-Type Voltage Responses from Hybrids of Carbon Nanotubes and Poly(3,4-ethylenedioxythiophene) with Tetrakis(dimethylamino)ethylene. *Advanced Materials* **2015,** *27* (43), 6855-6861.

27.   Mai, C. K.; Russ, B.; Fronk, S. L.; Hu, N.; Chan-Park, M. B.; Urban, J. J.; Segalman, R. A.; Chabinyc, M. L.; Bazan, G. C., Varying the Ionic Functionalities of Conjugated Polyelectrolytes Leads to Both p-and n-Type Carbon Nanotube Composites for Flexible Thermoelectrics. *Energy Environ. Sci.* **2015,** *8*, 2341.

28.   Fukumaru, T.; Fujigaya, T.; Nakashima, N., Development of n-type cobaltocene-encapsulated carbon nanotubes with remarkable thermoelectric property. *Scientific Reports* **2015,** *5*, 7951.

29.   Nonoguchi, Y.; Ohashi, K.; Kanazawa, R.; Ashiba, K.; Hata, K.; Nakagawa, T.; Adachi, C.; Tanase, T.; Kawai, T., Systematic Conversion of Single Walled Carbon Nanotubes into n-type Thermoelectric Materials by Molecular Dopants. *Scientific Reports* **2013,** *3*, 3344.

30.   Freeman, D. D.; Choi, K.; Yu, C., N-type thermoelectric performance of functionalized carbon nanotube-filled polymer composites. *PLoS One* **2012,** *7* (11), e47822-e47822.

31.   Blackburn, J. L.; Ferguson, A. J.; Cho, C.; Grunlan, J. C., Carbon-Nanotube-Based Thermoelectric Materials and Devices. *Advanced Materials* **2018,** *30* (11), 1704386.

32.   Taroni, P. J.; Santagiuliana, G.; Wan, K.; Calado, P.; Qiu, M.; Zhang, H.; Pugno, N. M.; Palma, M.; Stingelin-Stutzman, N.; Heeney, M.; Fenwick, O.; Baxendale, M.; Bilotti, E., Toward

Stretchable Self-Powered Sensors Based on the Thermoelectric Response of PEDOT:PSS/Polyurethane Blends. *Advanced Functional Materials* **2018,** *28* (15), 1704285.

33.   Fan, W.; Guo, C.-Y.; Chen, G., Flexible films of poly(3,4-ethylenedioxythiophene)/carbon nanotube thermoelectric composites prepared by dynamic 3-phase interfacial electropolymerization and subsequent physical mixing. *Journal of Materials Chemistry A* **2018,** *6* (26), 12275-12280.

34.   Zhao, J.; Tan, D.; Chen, G., A strategy to improve the thermoelectric performance of conducting polymer nanostructures. *Journal of Materials Chemistry C* **2017,** *5* (1), 47-53.

35.   Li, J.; Lai, C.; Xiang, X.; Wang, L., Synthesis and characterization of poly-Schiff bases with a donor–acceptor structure containing thiophene units as thermoelectric materials. *Journal of Materials Chemistry C* **2015,** *3* (11), 2693-2701.

36.   Li, Z.; Saini, V.; Dervishi, E.; Kunets, V. P.; Zhang, J.; Xu, Y.; Biris, A. R.; Salamo, G. J.; Biris, A. S., Polymer functionalized n-type single wall carbon nanotube photovoltaic devices. *Applied Physics Letters* **2010,** *96* (3), 033110.

37.   Javey, A.; Tu, R.; Farmer, D. B.; Guo, J.; Gordon, R. G.; Dai, H., High Performance n-Type Carbon Nanotube Field-Effect Transistors with Chemically Doped Contacts. *Nano Letters* **2005,** *5* (2), 345-348.

38.   Shim, M.; Javey, A.; Shi Kam, N. W.; Dai, H., Polymer Functionalization for Air-Stable n-Type Carbon Nanotube Field-Effect Transistors. *Journal of the American Chemical Society* **2001,** *123* (46), 11512-11513.

39.   Bradley, K.; Jhi, S.-H.; Collins, P. G.; Hone, J.; Cohen, M. L.; Louie, S. G.; Zettl, A., Is the Intrinsic Thermoelectric Power of Carbon Nanotubes Positive? *Physical Review Letters* **2000,** *85* (20), 4361-4364.

40.   Tan, D.; Zhao, J.; Gao, C.; Wang, H.; Chen, G.; Shi, D., Carbon Nanoparticle Hybrid Aerogels: 3D Double-Interconnected Network Porous Microstructure, Thermoelectric, and Solvent-Removal Functions. *ACS Applied Materials & Interfaces* **2017,** *9* (26), 21820-21828.

41.   Gao, C.; Chen, G., A new strategy to construct thermoelectric composites of SWCNTs and poly-Schiff bases with 1,4-diazabuta-1,3-diene structures acting as bidentate-chelating units. *Journal of Materials Chemistry A* **2016,** *4* (29), 11299-11306.

42.   Feng, N.; Gao, C.; Guo, C.-Y.; Chen, G., Copper-Phenylacetylide Nanobelt/Single-Walled Carbon Nanotube Composites: Mechanochromic Luminescence Phenomenon and Thermoelectric Performance. *ACS Applied Materials & Interfaces* **2018,** *10* (6), 5603-5608.

43.   Montgomery, D. S.; Hewitt, C. A.; Barbalace, R.; Jones, T.; Carroll, D. L., Spray doping method to create a low-profile high-density carbon nanotube thermoelectric generator. *Carbon* **2016,** *96*, 778-781.

44.   Hewitt, C. A.; Montgomery, D. S.; Barbalace, R. L.; Carlson, R. D.; Carroll, D. L., Improved thermoelectric power output from multilayered polyethylenimine doped carbon nanotube based organic composites. *Journal of Applied Physics* **2014,** *115* (18), 184502.

45.   Wu, G.; Zhang, Z.-G.; Li, Y.; Gao, C.; Wang, X.; Chen, G., Exploring High-Performance n-Type Thermoelectric Composites Using Amino-Substituted Rylene Dimides and Carbon Nanotubes. *ACS Nano* **2017,** *11* (6), 5746-5752.

46.   Brownlie, L.; Shapter, J., Advances in carbon nanotube n-type doping: Methods, analysis and applications. *Carbon* **2018,** *126*, 257-270.

47.   Piao, M.; Na, J.; Choi, J.; Kim, J.; Kennedy, G. P.; Kim, G.; Roth, S.; Dettlaff-Weglikowska, U., Increasing the thermoelectric power generated by composite films using chemically functionalized single-walled carbon nanotubes. *Carbon* **2013,** *62*, 430-437.

48.   Chang, C.-Y.; Huang, W.-K.; Chang, Y.-C.; Lee, K.-T.; Chen, C.-T., A solution-processed n-doped fullerene cathode interfacial layer for efficient and stable large-area perovskite solar cells. *Journal of Materials Chemistry A* **2016,** *4* (2), 640-648.

49.   Wu, G.; Gao, C.; Chen, G.; Wang, X.; Wang, H., High-performance organic thermoelectric modules based on flexible films of a novel n-type single-walled carbon nanotube. *Journal of Materials Chemistry A* **2016,** *4* (37), 14187-14193.

50.   Nonoguchi, Y.; Nakano, M.; Murayama, T.; Hagino, H.; Hama, S.; Miyazaki, K.; Matsubara, R.; Nakamura, M.; Kawai, T., Simple Salt-Coordinated n-Type Nanocarbon Materials Stable in Air. *Adv. Funct. Mater.* **2016,** *26*, 3021.

51.   Hewitt, C. A.; Kaiser, A. B.; Roth, S.; Craps, M.; Czerw, R.; Carroll, D. L., Multilayered Carbon Nanotube/Polymer Composite Based Thermoelectric Fabrics. *Nano Lett.* **2012,** *12*, 1307.

52.   Minnich, A. J.; Dresselhaus, M. S.; Ren, Z. F.; Chen, G., Bulk nanostructured thermoelectric materials: current research and future prospects. *Energy & Environmental Science* **2009,** *2* (5), 466-479.

53.   Yu, C.; Murali, A.; Choi, K.; Ryu, Y., Air-stable fabric thermoelectric modules made of N- and P-type carbon nanotubes. *Energy & Environmental Science* **2012,** *5* (11), 9481-9486.

54.   Mistry, K. S.; Larsen, B. A.; Bergeson, J. D.; Barnes, T. M.; Teeter, G.; Engtrakul, C.; Blackburn, J. L., n-Type Transparent Conducting Films of Small Molecule and Polymer Amine Doped Single-Walled Carbon Nanotubes. *ACS Nano* **2011,** *5* (5), 3714-3723.

55.   Li, L.-J.; Khlobystov, A. N.; Wiltshire, J. G.; Briggs, G. A. D.; Nicholas, R. J., Diameter-selective encapsulation of metallocenes in single-walled carbon nanotubes. *Nature Materials* **2005,** *4* (6), 481-485.

56.   Kim, S. L.; Choi, K.; Tazebay, A.; Yu, C., Flexible Power Fabrics Made of Carbon Nanotubes for Harvesting Thermoelectricity. *ACS Nano* **2014,** *8* (3), 2377-2386.

57.   Cheng, X.; Wang, X.; Chen, G., A convenient and highly tunable way to n-type carbon nanotube thermoelectric composite film using common alkylammonium cationic surfactant. *Journal of Materials Chemistry A* **2018,** *6* (39), 19030-19037.

58.   Kipphan, H., Handbook of Print Media. In *Handbook of Print Media*, Springer: Heidelberg, Germany, 2001; pp 1-202.

59.   Suganuma, K., *Introduction to Printed Electronics*. Springer: Osaka , Japan, 2014.

60.   Park, J.; Kim, S.; Lee, C., An Analysis of Pinned Edge Layer of Slot-Die Coated Film in Roll-to-Roll Green Manufacturing System. *International Journal of Precision Engineering and Manufacturing-Green Technology* **2018,** *5* (2), 247-254.

61.   Choi, J.; Jung, Y.; Yang, S. J.; Oh, J. Y.; Oh, J.; Jo, K.; Son, J. G.; Moon, S. E.; Park, C. R.; Kim, H., Flexible and Robust Thermoelectric Generators Based on All-Carbon Nanotube Yarn without Metal Electrodes. *ACS Nano* **2017,** *11* (8), 7608-7614.

62.   Collins, P. G.; Bradley, K.; Ishigami, M.; Zettl, A., Extreme Oxygen Sensitivity of Electronic Properties of Carbon Nanotubes. *Science* **2000,** *287* (5459), 1801.

63.   Blackburn, J. L.; Barnes, T. M.; Beard, M. C.; Kim, Y.-H.; Tenent, R. C.; McDonald, T. J.; To, B.; Coutts, T. J.; Heben, M. J., Transparent Conductive Single-Walled Carbon Nanotube Networks with Precisely Tunable Ratios of Semiconducting and Metallic Nanotubes. *ACS Nano* **2008,** *2* (6), 1266-1274.

64.   Tenent, R. C.; Barnes, T. M.; Bergeson, J. D.; Ferguson, A. J.; To, B.; Gedvilas, L. M.; Heben, M. J.; Blackburn, J. L., Ultrasmooth, Large-Area, High-Uniformity, Conductive Transparent Single-Walled-Carbon-Nanotube Films for Photovoltaics Produced by Ultrasonic Spraying. *Advanced Materials* **2009,** *21* (31), 3210-3216.

65.   Zhou, W.; Vavro, J.; Nemes, N. M.; Fischer, J. E.; Borondics, F.; Kamarás, K.; Tanner, D. B., Charge transfer and Fermi level shift in p-doped single-walled carbon nanotubes. *Physical Review B* **2005,** *71* (20), 205423.

66.   Zhou, W.; Fan, Q.; Zhang, Q.; Cai, L.; Li, K.; Gu, X.; Yang, F.; Zhang, N.; Wang, Y.; Liu, H.; Zhou, W.; Xie, S., High-performance and compact-designed flexible thermoelectric modules enabled by a reticulate carbon nanotube architecture. *Nature Communications* **2017,** *8* (1), 14886.

67.   Tzounis, L., Organic Thermoelectrics and Thermoelectric Generators (TEGs) In *Advanced Thermoelectric Materials for Energy Harvesting Applications*, IntechOpen: 2019.

68.   Dresselhaus, M. S.; Dresselhaus, G.; Saito, R.; Jorio, A., Raman spectroscopy of carbon nanotubes. *Physics Reports* **2005,** *409* (2), 47-99.

69.   Kazaoui, S.; Minami, N.; Jacquemin, R.; Kataura, H.; Achiba, Y., Amphoteric doping of single-wall carbon-nanotube thin films as probed by optical absorption spectroscopy. *Physical Review B* **1999,** *60* (19), 13339-13342.

70.   Wu, Z.; Chen, Z.; Du, X.; Logan, J. M.; Sippel, J.; Nikolou, M.; Kamaras, K.; Reynolds, J. R.; Tanner, D. B.; Hebard, A. F.; Rinzler, A. G., Transparent, Conductive Carbon Nanotube Films. *Science* **2004,** *305* (5688), 1273.

71.   Santhosh, P. B.; Thomas, N.; Sudhakar, S.; Chadha, A.; Mani, E., Phospholipid stabilized gold nanorods: towards improved colloidal stability and biocompatibility. *Physical Chemistry Chemical Physics* **2017,** *19* (28), 18494-18504.

72.   Wang, B.; Zhou, M.; Rozynek, Z.; Fossum, J. O., Electrorheological properties of organically modified nanolayered laponite: influence of intercalation, adsorption and wettability. *Journal of Materials Chemistry* **2009,** *19* (13), 1816-1828.

73.   King, S. G.; McCafferty, L.; Stolojan, V.; Silva, S. R. P., Highly aligned arrays of super resilient carbon nanotubes by steam purification. *Carbon* **2015,** *84*, 130-137.

74.   Geng, H.-Z.; Kim, K. K.; So, K. P.; Lee, Y. S.; Chang, Y.; Lee, Y. H., Effect of Acid Treatment on Carbon Nanotube-Based Flexible Transparent Conducting Films. *Journal of the American Chemical Society* **2007,** *129* (25), 7758-7759.

75.   Nouri, H.; Zouzou, N.; Moreau, E.; Dascalescu, L.; Zebboudj, Y., Effect of relative humidity on current–voltage characteristics of an electrostatic precipitator. *Journal of Electrostatics* **2012,** *70* (1), 20-24.

76.   Korotcenkov, G., *Handbook of Humidity Measurement: Methods, Materials and Technologies, Vol. 2: Electronic and Electrical Humidity Sensors*. 2019.

77.   Kharissova, O.; Kharisov, B., *Solubilization and Dispersion of Carbon Nanotubes*. Springer Nature: 2017.

78.   Xu, X.; Andresen, J.; Song, C.; Miller, B.; Scaroni, A. W., Preparation of novel CO2 "molecular basket" of polymer modified MCM-41. *ACS Division of Fuel Chemistry, Preprints* **2002,** *47*, 67-68.

79.   Temizer, İ.; İlkılıç, C., The performance and analysis of the thermoelectric generator system used in diesel engines. *Renewable and Sustainable Energy Reviews* **2016,** *63*, 141-151.

80.   Snyder, G. J.; Snyder, A. H., Figure of merit ZT of a thermoelectric device defined from materials properties. *Energy & Environmental Science* **2017,** *10* (11), 2280-2283.

81.   Snyder, G. J.; Toberer, E. S., Complex thermoelectric materials. *Nature Materials* **2008,** *7* (2), 105-114.

82.   Salvador, J. R.; Cho, J. Y.; Ye, Z.; Moczygemba, J. E.; Thompson, A. J.; Sharp, J. W.; Koenig, J. D.; Maloney, R.; Thompson, T.; Sakamoto, J.; Wang, H.; Wereszczak, A. A.,

Conversion efficiency of skutterudite-based thermoelectric modules. *Physical Chemistry Chemical Physics* **2014,** *16* (24), 12510-12520.

83. Prasher, R. S.; Hu, X. J.; Chalopin, Y.; Mingo, N.; Lofgreen, K.; Volz, S.; Cleri, F.; Keblinski, P., Turning Carbon Nanotubes from Exceptional Heat Conductors into Insulators. *Physical Review Letters* **2009,** *102* (10), 105901.

84. Grujicic, M.; Cao, G.; Roy, W., Computational analysis of the lattice contribution to thermal conductivity of single-walled carbon nanotubes. *Journal of Materials Science* **2005,** *40*, 1943-1952.

85. Lan, Y.; Wang, Y.; Ren, Z., Physics and applications of aligned carbon nanotubes. *Advances in Physics - ADVAN PHYS* **2011,** *60*, 553-678.

86. Cowen, L.; Atoyo, J.; Carnie, M.; Baran, D.; Schroeder, B., Review—Organic Materials for Thermoelectric Energy Generation. *ECS Journal of Solid State Science and Technology* **2017,** *6*, N3080-N3088.

87. Wang, H.; Yu, C., Organic Thermoelectrics: Materials Preparation, Performance Optimization, and Device Integration. *Joule* **2019,** *3* (1), 53-80.

88. Lu, Y.; Ding, Y.; Qiu, Y.; Cai, K.; Yao, Q.; Song, H.; Tong, L.; He, J.; Chen, L., Good Performance and Flexible PEDOT:PSS/Cu2Se Nanowire Thermoelectric Composite Films. *ACS Applied Materials & Interfaces* **2019,** *11* (13), 12819-12829.

89. Lu, Y.; Qiu, Y.; Jiang, Q.; Cai, K.; Du, Y.; Song, H.; Gao, M.; Huang, C.; He, J.; Hu, D., Preparation and Characterization of Te/Poly(3,4-ethylenedioxythiophene):Poly(styrenesulfonate)/Cu7Te4 Ternary Composite Films for Flexible Thermoelectric Power Generator. *ACS Applied Materials & Interfaces* **2018,** *10* (49), 42310-42319.

90. Wang, L.; Yao, Q.; Shi, W.; Qu, S.; Chen, L., Engineering carrier scattering at the interfaces in polyaniline based nanocomposites for high thermoelectric performances. *Mater. Chem. Front.* **2017,** *1*.

91. Tian, R.; Wan, C.; Wang, Y.; Wei, Q.; Ishida, T.; Yamamoto, A.; Tsuruta, A.; Shin, W.; Li, S.; Koumoto, K., A solution-processed TiS2/organic hybrid superlattice film towards flexible thermoelectric devices. *Journal of Materials Chemistry A* **2017,** *5* (2), 564-570.

92. Choi, J.; Lee, J. Y.; Lee, S.-S.; Park, C. R.; Kim, H., High-Performance Thermoelectric Paper Based on Double Carrier-Filtering Processes at Nanowire Heterojunctions. *Advanced Energy Materials* **2016,** *6* (9), 1502181.

93. Suarez, F.; Nozariasbmarz, A.; Vashaee, D.; Öztürk, M. C., Designing thermoelectric generators for self-powered wearable electronics. *Energy & Environmental Science* **2016,** *9* (6), 2099-2113.

94. Zeng, W.; Tao, X.-M.; Lin, S.; Lee, C.; Shi, D.; Lam, K.-h.; Huang, B.; Wang, Q.; Zhao, Y., Defect-engineered reduced graphene oxide sheets with high electric conductivity and controlled thermal conductivity for soft and flexible wearable thermoelectric generators. *Nano Energy* **2018,** *54*, 163-174.

95. Kim, C. S.; Lee, G. S.; Choi, H.; Kim, Y. J.; Yang, H. M.; Lim, S. H.; Lee, S.-G.; Cho, B. J., Structural design of a flexible thermoelectric power generator for wearable applications. *Applied Energy* **2018,** *214*, 131-138.

96. Park, K. T.; Choi, J.; Lee, B.; Ko, Y.; Jo, K.; Lee, Y. M.; Lim, J. A.; Park, C. R.; Kim, H., High-performance thermoelectric bracelet based on carbon nanotube ink printed directly onto a flexible cable. *Journal of Materials Chemistry A* **2018,** *6* (40), 19727-19734.

97.   Lindorf, M.; Mazzio, K. A.; Pflaum, J.; Nielsch, K.; Brütting, W.; Albrecht, M., Organic-based thermoelectrics. *Journal of Materials Chemistry A* **2020,** *8* (16), 7495-7507.

98.   Liu, J.; van der Zee, B.; Alessandri, R.; Sami, S.; Dong, J.; Nugraha, M. I.; Barker, A. J.; Rousseva, S.; Qiu, L.; Qiu, X.; Klasen, N.; Chiechi, R. C.; Baran, D.; Caironi, M.; Anthopoulos, T. D.; Portale, G.; Havenith, R. W. A.; Marrink, S. J.; Hummelen, J. C.; Koster, L. J. A., N-type organic thermoelectrics: demonstration of ZT > 0.3. *Nature Communications* **2020,** *11* (1), 5694.